GEOSTANDARDS and GEOANALYTICAL RESEARCH

Determination of Ultra-Trace Au, Ag, As, Pt and Re Mass Fractions in Volcanic Glasses and Rock Powders by LA-ICP-MS

Thomas M. **Belgrano*** , James A. **Milton** and Damon A.H. **Teagle**

School of Ocean and Earth Science, National Oceanography Centre Southampton, University of Southampton, European Way, Southampton SO14 3ZH, UK

* Corresponding author. e-mail: t.belgrano@soton.ac.uk

Practical methods for determining the ultra-trace abundances of precious metals in geological materials are needed for research into magmatic and hydrothermal processes and to expand the geochemical footprints of concealed ore deposits. This study presents a new protocol for determining Au, Ag, As, Pt and Re mass fractions in both volcanic glasses and in rock powders prepared as nano-powder pellets, through the synthesis and refinement of published LA-ICP-MS methods. This matrix flexibility allows the method and its limitations to be rigorously assessed for the first time using different volcanic materials. High-yield laser parameters, interference corrections and low oxide production rates facilitated by laser ablation sampling enabled accurate measurements without chemical pre-separation. A key finding is that ablation-remobilised system contamination must be quantified and corrected to make accurate ng g^{-1}-level Au determinations by LA-ICP-MS, resulting in a mean + 2*s* quantification limit for Au of 0.38 ng g^{-1}. This approach is likely necessary for other ultra-trace LA-ICP-MS analyses of certain elements. Following this correction, the protocol can be usefully applied to both *in situ* analysis of volcanic materials and efficiently integrated into methods for the determination of major and trace elements in nano-powder pellets.

Keywords: gold, PGE, LA-ICP-MS, silver, arsenic, nano-pellet.

Received 05 Jan 22 – Accepted 07 Jul 22

Practical methods for the determination of ultra-trace mass fractions of precious metals such as Au, Ag, Pt and Re in rock samples are an enduring challenge to analytical geochemistry and a persistent limitation on ore deposit research and exploration (e.g., Crocket *et al.* 1968, Cameron 1989, Pitcairn *et al.* 2006, Constantin 2009, Braukmüller *et al.* 2020, Liu *et al.* 2020). *In situ* methods have advantages for the characterisation of natural and experimental glasses and minerals but microanalysis of precious metal concentrations in silicate samples, such as by LA-ICP-MS, presents additional challenges (e.g., Sylvester and Eggins 1997, Jenner and O'Neill 2012b, Schlöglova *et al.* 2017). However, if such *in situ* approaches can be demonstrated to be efficacious, they could be routinely applied to large numbers of whole rock samples prepared as nano-powder pellets for conventional major and trace element analysis (Garbe-Schönberg and Müller 2014, Peters and Pettke 2016).

The analytical challenges arise from the low abundances of Au, Pt, Re (~ 0.1 to 10 ng g^{-1}) and Ag (~ 10 to 100 ng g^{-1}) in typical crustal and mantle rocks, combined with polyatomic, isobaric ICP-MS interferences of $^{181}Ta^{16}O$ and $^{180}Hf^{16}O^{1}H$ on ^{197}Au, $^{179}Hf^{16}O$ on ^{95}Pt, $^{91}Zr^{16}O$ on ^{107}Ag and $^{93}Nb^{16}O$ and $^{92}Zr^{16}O^{1}H$ on ^{109}Ag. Accurate ICP-MS measurement of ^{75}As is similarly impeded by $^{40}Ar^{35}Cl$ and doubly charged $^{150}Sm^{2+}$ and $^{150}Nd^{2+}$ interferences. These challenges are compounded with a high potential for contamination from remobilisation of previously ablated material from the laser ablation system and tubing (Schlöglova *et al.* 2017), the irregular distribution of Au in rocks, requiring larger representative sample masses than most other elements (i.e., 'the nugget effect'; Pitcairn *et al.* 2006) and documented heterogeneity of these elements in NIST SRM 61x 'external' calibration glasses (Eggins and Shelley 2002).

doi: 10.1111/ggr.12452

Problematic interferences have conventionally been overcome for solution ICP-MS approaches by chemical separation of the analytes from the interfering elements (e.g., Cheng *et al.* 2019, Oguri *et al.* 1999, Pitcairn *et al.* 2006, Tao *et al.* 2017). More recently, tandem mass spectrometry (MS/MS) methods utilising reactive gases to separate interferences online have allowed whole rock digestions to be measured without pre-separation of interferences, resulting in new, high throughput protocols for elements such as Au, Ag, S, As, Se, Rh, Pd (e.g., Yim *et al.* 2012, Sugiyama and Shikamori 2015, Yang *et al.* 2020, Hammond *et al.* 2021, Sugiyama 2021). However, for LA-ICP-MS analysis chemical pre-separation of elements affected by interferences is not possible. Online interference elimination using LA-ICP-MS/MS is feasible for some elements (e.g., Se; Reekie *et al.* 2019), but the gas reactions and collisions result in significantly reduced sensitivity that precludes the detection of Au, Pt and Re at naturally relevant mass fractions.

LA-ICP-MS measurement of Au, Ag, As, Pt and Re

The *in situ* capability of LA-ICP-MS is necessary for studies of many natural and experimental volcanic glasses and minerals, where target minerals may be zoned or incipient alteration needs to be avoided. Nano-particulate powder pellets also allow LA-ICP-MS to be applied to whole-rock powder analysis, eliminating issues related to acid safety and incomplete digestion while permitting simultaneous determination of major and trace elements (Garbe-Schönberg and Müller 2014, Peters and Pettke 2016). The method and assessments detailed in this study are primarily aimed at these two use cases: *in situ* precious metal analysis of volcanic glasses, and the cost- and time-efficient addition of precious metals analysis to analytical workflows for major and trace elements in nano-powder pellets.

Crucial components of this method have been established over the past two decades. Sylvester and Eggins (1997) determined the mass fractions of Au and platinum group elements (PGE) in NIST SRM 61x glasses by isotope dilution ICP-MS and used these values to calibrate LA-ICP-MS analyses of the NIST glasses as well as two natural basaltic glasses. Interference production rates measured on baddeleyite and spiked synthetic glasses were used to make offline interference corrections. To achieve adequate sensitivity, laser parameters of a 200μm laser spot size and a 50 Hz repetition rate was employed, resulting in a reported detection limit for Au of 0.29 ng g^{-1}, calculated after Longerich *et al.* (1996). Collections of volcanic glasses have since been analysed for Au, Ag, As, Pt and Re by LA-ICP-MS (Norman *et al.* 2004, Sun *et al.* 2004, Jenner and O'Neill 2012a), generally utilising a large laser spot diameter of 190–250 μm, a laser repetition rate of 15–20 Hz, and various minerals and doped glasses for interference monitoring and correction. With calculated detection limits for Au as low as 0.25 ng g^{-1}, Pt of 0.2 ng g^{-1} and Re of 0.05 ng g^{-1}, these datasets demonstrate the utility of the technique for studying natural magmatic systems. The influence of various tuning parameters on Au and Pt sensitivity and oxide production rates during LA-ICP-MS were explored in detail by Hu *et al.* (2009). Although that study focused on synthetic glasses with relatively high Au and PGE mass fractions, the results show that post-chamber additions of N_2 at 5 ml min^{-1} and plasma sampling depths of ~ 5 mm provide reasonable Au sensitivity at low oxide production rates.

These previous studies were pioneering and rigorous. However, what they and the broader community have lacked are microanalytical reference materials with suitably 'natural' Au, Ag, Pt and Re mass fractions to properly assess the method. Potentially relevant but accordingly untested sources of error include the matrix effect on oxide production rates measured on different materials (Gilbert *et al.* 2017), laser induced elemental fractionation (Jenner and O'Neill 2012b) and memory effects (Jenner and O'Neill 2012b, Schlöglova et al. 2017).

This study will synthesise previous LA-ICP-MS developments into a practical protocol with a particular emphasis on Au, quantitatively assess its performance and limitations including potential sources of error, and assess whether the nano-powder pellet production process can sufficiently homogenise rock powders for meaningful precious metals analyses. Accuracy is assessed down to the ng g^{-1} to sub-ng g^{-1} level using a combination of international basaltic to andesitic reference powders prepared as nano-powder pellets as well as mid-ocean ridge basalt (MORB) glasses with Au values determined precisely by Webber *et al.* (2013). The utility of the method is demonstrated by providing new results for additional reference glasses and powder reference materials. Effective quantification limits for the method are discussed, along with the advantages and disadvantages of sample introduction via laser ablation and potential applicability in research and commercial settings.

Reference materials and preparation

The method presented here requires a set of specialised but intentionally accessible materials. For external calibration and performance monitoring, NIST SRM 616–612 glasses were used, with reference values taken from Jochum *et al.* (2011). Minerals and one synthetic basaltic glass

(RK54_SM1) were used to quantify interferences and instrumental blanks. The minerals used were natural zircon, tantalite, halite, San Carlos olivine and synthetic quartz. The RK54_SM1 basaltic glass was synthesised at ETH Zürich in a Pt-Pd capsule and doped with ~ 30–40 μg g^{-1} of lithophile elements including Sm and Nd (Marxer *et al.* 2022). Despite no intentional chalcophile element additions to RK54_SM1, it is contaminated by Pt, Re, Au and Ag from synthesis in PGE capsules (see also Eggins and Shelley 2002). Consequently RK54_SMI could only be used for correcting interferences on As.

Nano-particulate powders of the USGS powder reference materials BIR-1, BHVO-2, BCR-2 and AGV-2 were produced at the University of Bern following Peters and Pettke (2016). Briefly summarised here, 2.2 g of each powder was milled with 5.6 g of Milli-Q ultrapure water (Merck KGaA, Darmstadt, Germany) and 36 g of 7 mm agate balls in a 50 ml agate vial in a Retsch (Haan, Germany) PM100 planetary ball mill for 22 min at 600 Hz, then dried down at 50 °C. At the University of Southampton, this dried powder was re-homogenised in an agate hand mortar, then 400 mg was combined with 40 mg of micro-crystalline cellulose binder (PN310697, SigmaAldrich, Saint Louis, USA), homogenised again in an agate hand mortar and pressed into a 13 mm diameter pellet in a stainless-steel pellet die (Specac, Kent, UK) at 10 MPa for 10 min. This binder to sample mass ratio (1:10) is half of that used by Peters and Pettke (2016) and hence intermediate to the binder-free pellets of Garbe-Schönberg and Müller (2014). This ratio was chosen to reduce matrix differences between the pellets and glasses while retaining pellet cohesion. One additional, binder-free pellet of Geological Survey of Japan (GSJ) reference powder JB-3 was produced from 2 g of powder at the University of Southampton using the same method and Fritsch GmbH (Idar Oberstein, Germany) agate equipment as Garbe-Schönberg and Müller (2014).

For further assessment of ultra-trace Au accuracy, six natural MORB glasses from the Reykjanes Ridge with Au mass fractions between 0.20–4.26 ng g^{-1} previously determined by Webber *et al.* (2013) using the ultra-low detection limit method of Pitcairn *et al.* (2006). These glasses have previously had their major, trace element and Sr–Nd–Pb–He isotopic compositions characterised (Taylor *et al.* 1997, Murton *et al.* 2002). Glass samples were selected for their range in Au contents and their fresh, phenocryst-poor appearance. Several glass chips from each sample were mounted in epoxy for LA-ICP-MS analysis.

Method

Instrumental conditions and tuning

All analyses were performed by LA-ICP-MS in the Geochemistry Research Group Laboratories at the University of Southampton using an Agilent (Santa Clara, California) 8900 Triple Quadrupole ICP-MS coupled to an NWR193 excimer laser ablation system with a TwoVol2 ablation chamber (Elemental Scientific Lasers, Bozeman, USA). The key instrument and laser conditions are listed in Table 1. Two main laser ablation settings were used for measurements: 'high yield' to maximise sensitivity for natural materials with low analyte abundances and 'reduced yield' to reduce system contamination for synthetic glasses doped or contaminated with the analytes. Additional, even lower yield parameters were used for the minerals measured for interference corrections to avoid detector saturation for interfering elements (Table 1). Laser energy was set at 50% on the ESL software, translating to ~ 2 J cm^{-2} fluence at the sample. This relatively low fluence combined with higher laser repetition rates produces smooth ablations and high sensitivity on this system.

Pulse/analogue detector factors were determined in solution mode prior to laser ablation analysis sessions. Instrument tuning was carried out using 25 μm-wide line scan ablations of NIST SRM 612, optimised to maximise Au and Ag sensitivity, minimise oxide production rates, and maintain a U/Th ratio of 1 ± 0.05. Guided by the findings of Hu *et al.* (2009), nebuliser Ar flow, He carrier gas flow, post-chamber N_2 and plasma-sampling depth were the main parameters adjusted (Figure 1). The post-chamber addition of N_2 increases sensitivity at low oxide production conditions (Hu *et al.* 2009) and an optimum sensitivity was achieved at 6 ml min.

Initial attempts using O_2 and H_2 reaction modes to resolve or reduce various polyatomic interferences (e.g., Sugiyama 2021, Yim *et al.* 2012) reduced sensitivity for Au, Re and Pt to unacceptable levels. Proceeding in 'no-gas mode', an effective balance of Au sensitivity and oxide production rate was found (Table 1). Optimal conditions are similar to Hu *et al.* (2009). Although sensitivity and oxide production rates varied somewhat from session to session (e.g., ThO/Th = 0.050–0.075%), these parameters produced an optimal balance of sensitivity and oxide production rates while maintaining robust plasma conditions with a mean U/Th ratio of 103.6 ± 1.6 % (±2*s*, *n* = 4) for NIST SRM 612.

Table 1.
Instrumental and analytical conditions

Elemental Scientific Lasers NWR193			
Laser	193 nm Excimer		
Pulse width	7 ns		
Laser energy setting	50%		
Fluence at sample	~ 2 J cm^{-2}		
Ablation parameters	Spot (μm)	Repetition Rate (Hz)	Time (s)
High yield: pellets, MORB glasses, blanks, SRM614–616	150	40	50
Reduced yield: SRM612, RK and USGS glasses	90	20	40
Zircon, tantalite, halite	10–20	5	20
Agilent 8900 Triple Quadrupole ICP-MS			
Cones	Ni (Agilent)		
Reflected power	1550 W		
Plasma sampling depth	5 mm		
Reaction mode	No gas mode		
Ar gas flows	(l min^{-1})		
Nebuliser	0.63		
Plasma	15		
Auxiliary	0.9		
Carrier gases	(ml min^{-1})		
He (into chamber)	650		
N_2 (after chamber, via mixing bulb)	6		
Measured isotopes and detector dwell times	(ms)		
^{29}Si,^{35}Cl, ^{43}Ca, ^{91}Zr, ^{146}Nd, ^{147}Sm, ^{178}Hf, ^{181}Ta	10		
^{107}Ag	40		
^{185}Re, ^{195}Pt, ^{197}Au	60		

Measurement strategy

To reduce oxide production rates following sample changes, the chamber was bypassed from the ICP-MS and purged with He at 2 l min^{-1} for 5 min, then reconnected and the system flushed at normal gas flow rates for at least two hours before commencing analysis. Studies of the NIST SRM 61x glass reference materials have revealed heterogeneity for all of the target analytes, occurring as depletion around the rims and in cryptic depleted internal domains (Eggins and Shelley 2002, Jochum *et al.* 2011). Aside from these domains, homogeneity of the analytes is sufficient for spot sizes greater than ~ 80 μm (Jochum *et al.* 2011). To avoid inadvertently ablating a depleted domain, areas of the NIST glasses were pre-screened for heterogeneity using shallow line scans of rectangular areas of ~ 0.3 by 0.8 mm (Figure 2). Thallium has been shown to be a sensitive monitor of such heterogeneity in the NIST glasses (Eggins and Shelley 2002) so Tl was added for the line scan test. The stage repositioning and direction reversal at the end of each row is accompanied by a characteristic double drop in intensity that is just an artefact and can be ignored (shaded out in Figure 2). Replicate spot ablations for calibration were then located within the pre-screened rectangle and spaced apart to further reduce the impact of any undetected depletion on calibration (e.g., with depth). For NIST SRM 614 the same high yield ablation parameters as for our samples were used but for NIST SRM 612 reduced yield laser parameters were used (Table 1).

Batches of about eight sample measurements, typically with six replicate measurements each, were bracketed by three ablations each of the NIST calibration reference materials. To allow the system to flush and to provide regular intervals for gas blank measurements, an interval of 90 s was left between ablations of different materials. Only the final 30 s of these intervals were used to fit the background intensities.

Quantification and correction of polyatomic interferences

Interference production rates measured during each session were used to apply offline corrections to the entire

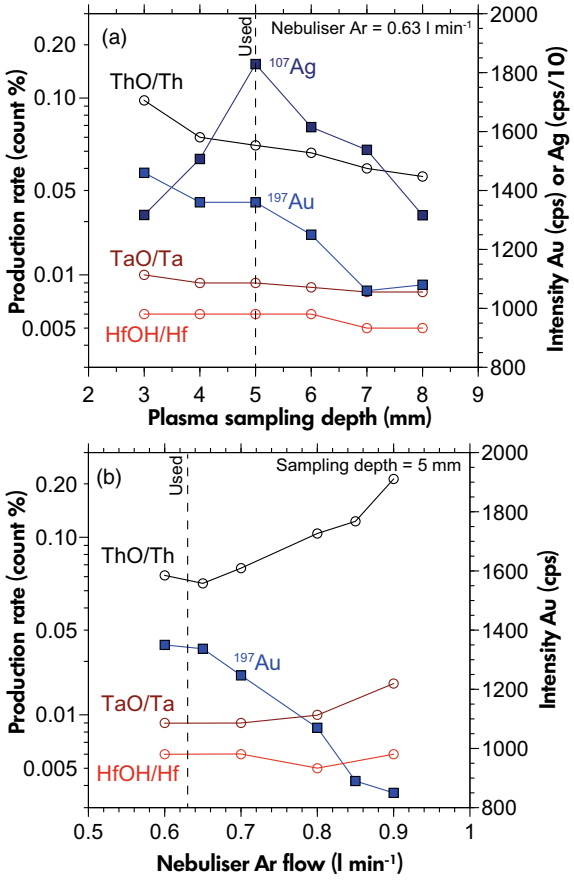

Figure 1. Oxide production rates and ^{197}Au and ^{107}Ag intensity during tuning versus (a) plasma sampling depth at fixed 0.63 l min^{-1} nebuliser Ar flow and (b) nebuliser Ar flow at fixed 5 mm sample depth. Both tests were performed at 0.65 l min^{-1} carrier He and 6 ml min^{-1} post-chamber N_2.

batch before calibration to mass fractions, including all reference material, background and sample measurements. Interference corrections were applied to each individual cycle of the raw intensity data. Although analyte-free synthetic basaltic glasses would be best to make matrix-matched interference corrections (Gilbert *et al.* 2017), such glasses could not be easily obtained. Here we proceeded with more widely available minerals (Table 2) and anticipate that other laboratories will face the same issue. These minerals are assumed to contain negligible amounts of the analytes relative to the elements that form their interferences. Matrix-related differences in oxide production rates between the minerals and the measured volcanic materials are possible. However, previous results suggest that the differences between tantalite and zircon versus glass are relatively minor for Hf, Zr and Ta oxides (Gilbert *et al.* 2017). The additional uncertainty introduced by this matrix effect is proportional to the relative magnitude of the interference correction. Consequently, it is essential to minimise oxide production rates as much as possible.

Interferences were measured directly on mass, but isotopes of the 'parent' elements for each interference were selected to be free of isobaric interferences or to not saturate the detector. Intensities for the interfering isotopes were then recalculated with natural abundances where necessary (e.g., Hf, Sm, Nd; Table 2).

Production rates for $^{181}Ta^{16}O/^{181}Ta$ and $^{180}Hf^{16}O^{1}H/^{180}Hf$ were measured on natural tantalite and zircon respectively and were used to correct ^{197}Au. The production rate of $^{91}Zr^{16}O/^{91}Zr$ measured on zircon was used to correct ^{107}Ag. For the interferences on ^{75}As, production of $^{40}Ar^{35}Cl/^{35}Cl$ was measured on halite. However, doubly charged $^{150}Sm^{2+}$ and $^{150}Nd^{2+}$ interferences, could not be resolved individually because no Sm-bearing but Nd-free materials could be obtained, or *vice versa*. Instead, a combined correction was approximated with the production rate of ($^{150}Sm^{2+}$ + $^{150}Nd^{2+}$) / ($^{150}Sm^{+}$ + $^{150}Nd^{+}$) measured on the nominally As-free RK54_SM1 synthetic basaltic glass.

The production rate of $^{179}Hf^{16}O/^{179}Hf$, a potential interference on ^{195}Pt, was assessed on zircon. Problematically, the $^{179}Hf^{16}O$ intensity predicted by this rate in some natural samples occasionally exceeded the measured counts on *m/z* (mass/charge) 195. The apparent production rate was also twice that of $^{181}Ta^{16}O/^{181}Ta$, when it should be similar (Gilbert *et al.* 2017). No such overcorrections were observed for $^{180}Hf^{16}O^{1}H$ interference on ^{197}Au, even for the relatively high Hf/Au AGV-2. This suggests that this overcorrection may be limited to *m/z* 195 and unrelated to the $^{180}Hf^{16}O^{1}H$ interference. Assuming the zircon contains a negligible amount of Pt relative to Hf, this suggests either an unconsidered interference contributed to the counts on *m/z* 195 for the zircon, or that some aspect of the zircon matrix remobilised Pt contamination from within the chamber and interface tubing. As ^{179}Hf has a relatively low natural isotopic abundance (13.6%) and Hf contents are not correlated with the uncorrected Pt values in our measurements (Figure S1), we conclude that the $^{179}Hf^{16}O$ interference on Pt is either minor or negligible for the materials in this study and hence was better left uncorrected. This may not hold true for evolved materials with higher Hf/Pt ratios.

Oxide interference monitoring materials were each measured three times in two blocks bracketing each entire batch of measurements. Regardless of the flushing time following sample change, oxide production rates consistently

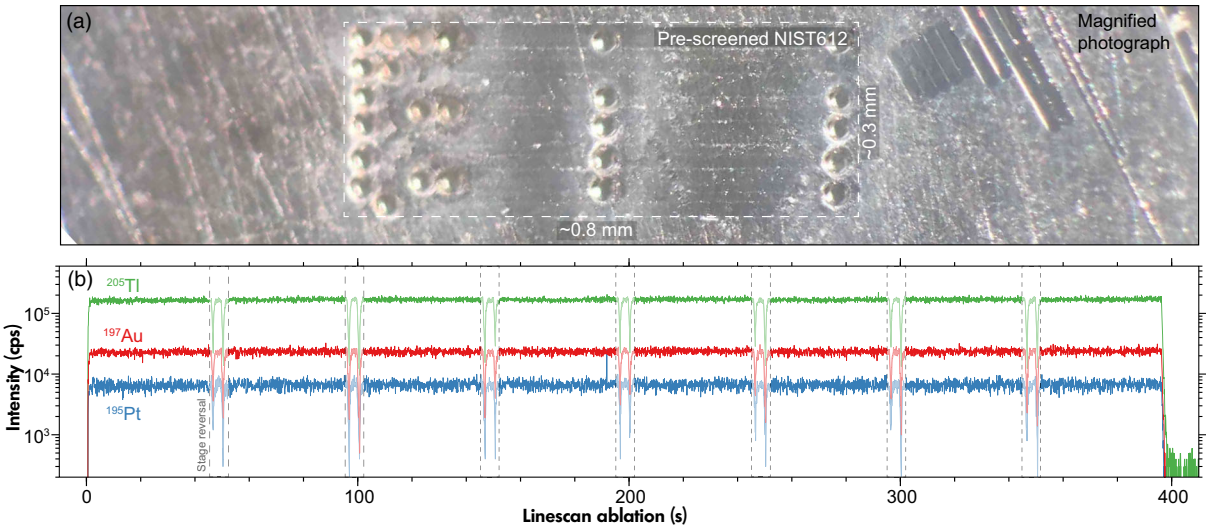

Figure 2. Example of pre-screening NIST calibration glasses for compositional heterogeneity. (a) Magnified photograph of NIST SRM 612 and pre-screened rectangle following rapid line scan ablation and several well-spaced calibration ablations. (b) Au, Pt, Tl intensity versus time during the line scan pictured in (a), regular intensity drops related to stage reversals are shaded.

Table 2.
Interferences monitored during this study

Analyte	Interference	Isotope monitored	Material	Recalculated ratio	Mean production rate (%)	2*s* (%)	Corrected (Yes/No)
^{197}Au	$^{181}Ta^{16}O^{+}$ $^{180}Hf^{16}O^{1}H^{+}$	^{181}Ta ^{178}Hf	Tantalite Zircon	$^{181}Ta^{16}O$ / ^{181}Ta $^{180}Hf^{16}O^{1}H$ / ^{180}Hf	0.0092 0.0061	0.0053 0.0030	Yes Yes
^{107}Ag	$^{91}Zr^{16}O^{+}$	^{91}Zr	Zircon	$^{91}Zr^{16}O$ / ^{91}Zr	0.0139	0.0034	Yes
^{75}As	$^{150}Sm^{2+}$ $^{150}Nd^{2+}$ $^{40}Ar^{35}Cl^{+}$	^{147}Sm ^{146}Nd ^{35}Cl	Doped glass Halite	$(^{150}Sm^{2+} + ^{150}Nd^{2+})$ / $(^{150}Sm^{+} + ^{150}Nd^{+})$ $^{40}Ar^{35}Cl/^{35}Cl$	1.38 0.009	0.12 0.017	Yes No
^{195}Pt	$^{179}Hf^{16}O^{+}$	^{178}Hf	Zircon	$^{179}Hf^{16}O^{+}$ /$^{179}Hf^{+}$	0.0222	0.0078	No

fell by 10–20% during each batch. For corrections, this reduction was approximated as a linear slope between the bracketing measurements at the beginning and end of each batch. Initial tests showed that doubly charged Sm^{2+} and Nd^{2+} production remained relatively constant during each batch and from session to session. Consequently, this rate was only measured once per batch to minimise the amount of Au-contaminated RK54_SM1 glass ablated.

Ablation-remobilised contamination and blank correction

Contamination remobilised during ablation from the sample chamber or tubing can produce spurious signals for certain elements such as Au, S and Cl that may be significant in comparison with the sample-derived signal (Guillong et al. 2008, Jenner and O'Neill 2012b, Schlöglova et al. 2017, Rottier and Audétat 2019). This signal, referred to as 'ablation-remobilised contamination', is not present in the gas blank and is thought to be generated by stray laser light hitting the contaminated inner sample chamber surfaces and abrasion of the contaminated chamber and tubing by the ablated aerosol, resulting in an excess signal that generally scales with ablation yield (Rottier and Audétat 2019).

Reduction and quantification of ablation-remobilised contamination is necessary for ultra-trace Au, which is both a particularly 'sticky' element and is several orders of magnitude more abundant in potential sources of contamination such as calibration glasses or sulfides than in typical igneous samples. We followed a simplified version of the steps

proposed by Schlöglova *et al.* (2017) for minimising ablation-remobilised Au contamination. Firstly, the ICP-MS cones, torch, mixing bulb and transfer lines were routinely extracted and cleaned. Unlike for Schlöglova *et al.* (2017) the sample chamber used for this study contains parts that cannot be cleaned with acid. Following these steps, mean gas background intensities for As were 150–350 cps and 25–100 cps for Ag. For Au, Re and Pt mean gas background intensities were < 1 cps. All of these gas backgrounds were straightforwardly fitted with a spline and subtracted from the signals in iolite4 prior to calibration.

Secondly, the ablation of NIST SRM 610 or other Au-rich materials was avoided entirely during and between sessions. The amount of NIST SRM 612 ablated during each session was also minimised wherever possible. For example, during instrument tuning, the minimum-yield settings necessary to achieve adequate ThO sensitivity were used. As the Au/Th ratio of NIST SRM 614 is higher than SRM 612, tuning with the latter can introduce less Au into the system. Reduced ablation-yield parameters were also used for NIST SRM 612 calibration measurements and the other synthetic glasses (Table 1). The first ablation of any natural material after an analyte-rich synthetic glass was discarded and each ablation site was pre-ablated for 2 s prior to measurement. Finally, a 10 s delay before the beginning of signal integration for each ablation allowed the highest and most variable ablation-remobilised contamination signals occurring in the first few seconds of ablation to flush through and for the signal to stabilise (e.g., San Carlos Olivine, Figure 3).

Despite these steps, residual ablation-remobilised contamination was present and needed to be quantified using a blank material in order to assess limits of quantification and to correct the analyses. Synthetic quartz has previously been used for this purpose (Schlöglova *et al.* 2017). Although well suited in terms of purity, quartz couples poorly with 193 nm laser light compared with mafic volcanic materials. This leads to drastically reduced ablation yields for quartz under the same laser settings and these reduced yields translate to reduced predictions of remobilised contamination (Rottier and Audétat 2019). Poor laser coupling may also produce large particulates by fracturing of the quartz, which would conversely lead to increased mobilisation of contamination within the chamber by abrasion. Consequently, quartz is an inappropriate ablation blank material for studies targeting materials that are not quartz.

Instead, a large natural crystal of San Carlos olivine was analysed during each batch (see also Jenner and O'Neill 2012b). The contamination signal measured with this blank is referred to as the 'ablation blank' and mass fractions were calibrated using Si as the internal standard element assuming 19% *m/m* Si (Fournelle 2011). San Carlos olivine was favoured over synthetic quartz because of its accessibility, its closer compositional match to the volcanic materials, its closely comparable ablation yields to glasses (Bussweiler *et al.* 2019), albeit under the assumption that it contains negligible amounts of the analytes. This assumption was not directly tested but is reasonable given the low concentrations of Au, Ag, Pt and Re (< 10 ng g^{-1}) and As (68 ± 20 ng g^{-1}) in primitive mantle (Palme and O'Neill 2014) and the extreme incompatibility of these elements in olivine, (e.g., olivine/melt partition coefficients of < 0.01 for Au, Ag, As, Pt and Re, Brenan *et al.* 2003, Brenan *et al.* 2005, Adam and Green 2006).

The ablation blank measured in olivine for each batch was subtracted as calibrated mass fractions from the interference-corrected values for Au, Ag and As. The 2*s* uncertainties of the final, blank corrected values were propagated by summing the 2*s* uncertainties of the replicate sample and blank measurements in quadrature. Neither Pt nor Re were corrected, as ablation-remobilised contamination was below detection for these elements.

Nano-powder pellet procedural blank

It has been shown using the same agate equipment as this study that contamination introduced during nano-powder pellet production is negligible for the vast majority of major and trace elements conventionally measured in igneous materials (Peters and Pettke 2016). Such contamination can be assessed by measuring a 'procedural blank', that is, the analyte mass fraction obtained for a matrix that does not contain the analyte but that was processed and analysed in the same manner as the samples. Nano-powder pellet procedural blank values have so far not been reported for Au, Ag, Pt or Re, or down to sub-ng g^{-1} levels in general. For this study, a procedural blank was measured following Peters and Pettke (2016), using high-purity synthetic quartz prepared and analysed in the same way as the powder reference materials, with intensities calibrated to a mass fraction with an internal standard of 100% *m/m* SiO_2.

Limits of detection and quantification

Limits of detection (LOD) were calculated in iolite4 following Pettke *et al.* (2012), taking into account the gas background intensity, analyte sensitivity, isotope dwell times and the number of integration cycles during each analysis. These detection limits are calculated using Poisson statistics, which are better suited to non-Gaussian intensity distributions at count rates approaching zero (Pettke *et al.* 2012).

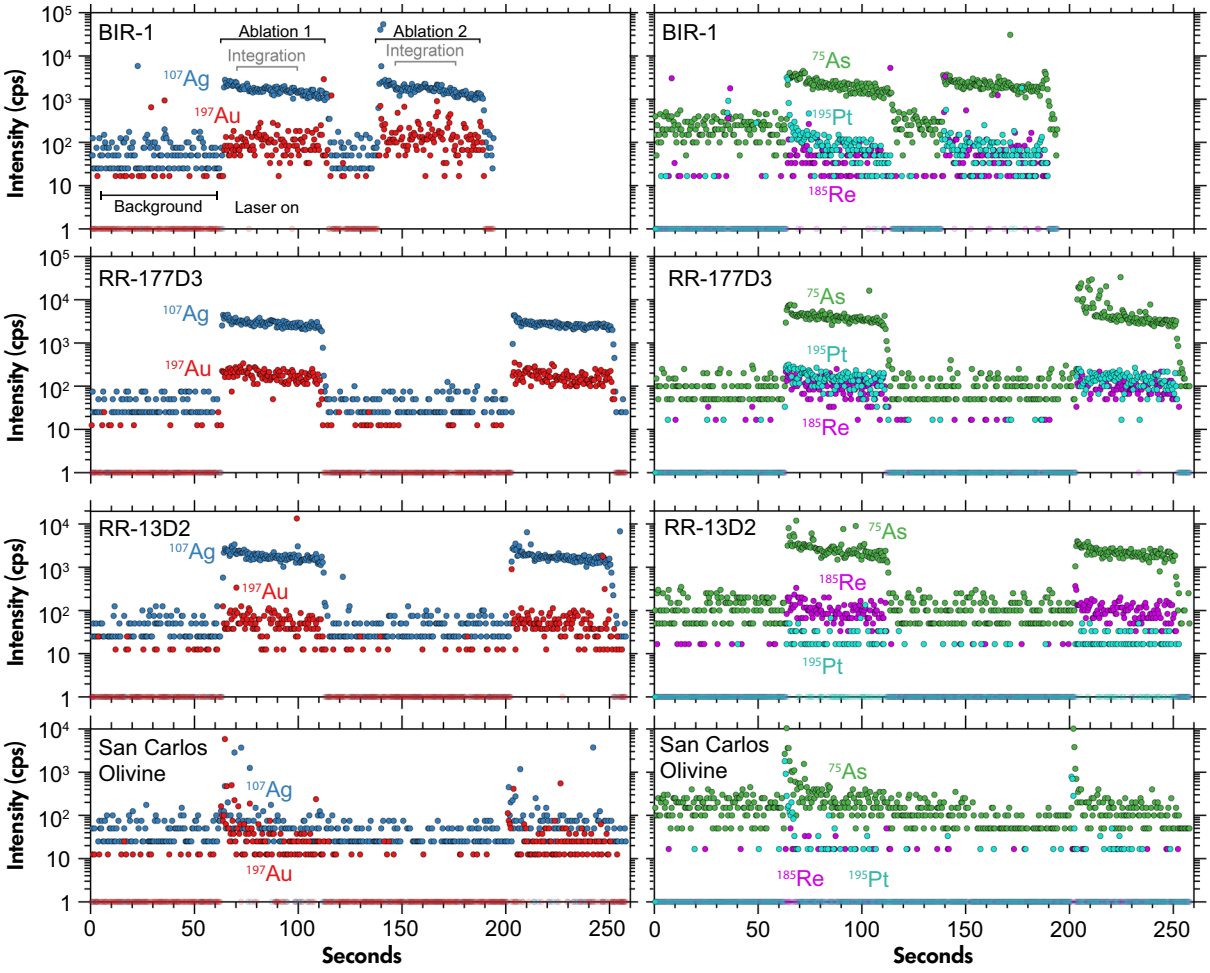

Figure 3. Raw LA-ICP-MS intensities for two consecutive ablations, with elements split into two columns for clarity. Intensities of 0 cps are shaded and plotted at 1 cps for visualisation on the log scale. (a) The BIR-1 nano-powder pellet, measured value for Au = 1.99 ± 0.94 ng g^{-1}, (b) the Reykjanes Ridge glass 177D3 (Au = 3.01 ± 0.30 ng g^{-1}), (c) the Reykjanes Ridge glass 13_D2 (Au = 0.66 ± 0.17 ng g^{-1}), (d) the San Carlos olivine blank.

For elements with ablation-remobilised contamination that exceeds the gas background, this contamination will exceed the LODs calculated following Pettke *et al.* (2012) or Longerich *et al.* (1996) (see Table 4). For these cases, the lowest mass fraction that can be reliably assigned to the sample is determined by the amount and variability of ablation-remobilised contamination, as quantified by the ablation blank. The method limit of quantification (LOQ) is defined as the mean + 2*s* of the ablation blank, above which the laser-remobilised contamination correction should be < 50% of the sample-derived mass fraction for ~ 95% of individual analyses.

Calibration to mass fractions

The interference corrected intensity data were calibrated to mass fractions in iolite4 software using the '3D Trace Elements' data reduction scheme (Paton *et al.* 2011, Petrus and Paul 2021). This scheme allows the sensitivity ratios of multiple reference materials to be yield-corrected and fitted with a calibration curve that can vary with instrumental drift during the session. A spline fit through the gas background-corrected origin, NIST SRM 614 and NIST SRM 612 produced the most accurate results for the reference materials measured. This approach combines the benefits of laser-parameter-matched high yield calibrations of NIST SRM 614 with reduced-yield and hence reduced contamination ablations of the higher-concentration NIST SRM 612. It also spreads the calibration weighting between two reference materials and more measurements per batch, reducing the potential error introduced by inadvertent ablations of heterogeneous NIST glass domains and further allowing these to be visually screened in the software using intensity versus concentration plots for each calibration block.

For calibration in iolite4, we elected to use median statistics with points falling outside of two median absolute deviations rejected as outliers. Median statistics were found to be more resistant to irregular positive spikes in intensity and more consistent between ablations for analytes measured close to the detection limit where ion intensity distributions become non-Gaussian (Pettke *et al.* 2012). Tests showed that internal standardisation using ^{43}Ca and ^{29}Si produce similar results. However, as Si could potentially be elevated in the nano-powders by milling in agate, we used ^{43}Ca for all the measured materials and ^{29}Si only for the Ca-poor blanks. Internal standard values for CaO were taken from the GeoReM preferred values for the reference materials (Jochum *et al.* 2005) and from Murton *et al.* (2002) for the Reykjanes Ridge glasses.

Assessment of plasma loading and matrix effects on oxide production

Tao *et al.* (2017) noted that the addition of CH_4 as a plasma modifier reduced HfOH and TaO production during solution ICP-MS. To assess whether organic C in the cellulose binder or other matrix differences could similarly affect oxide production rates, and hence interference corrections for pellets and glasses, we compared ThO/Th and UO/U in the BCR-2 nano-powder pellet and the BCR-2Ga glass, which otherwise have near-identical major element compositions (Table 3). The small difference in ThO/Th and the identical UO/U between the different BCR-2 matrices demonstrate that there is no substantial difference in oxide production rates between cellulose-bound powder pellets and glasses of the same composition. However, the difference between the basalts and NIST SRM 614 is far greater, with oxide production rates measured in either of the NIST glasses consistently ~ 40–50% higher than in a basaltic glass, although the mechanism behind this discrepancy is unknown.

Under the high yield ablation parameters necessary to achieve adequate Au and PGE sensitivity, plasma loading could potentially lead to decreasing atomisation efficiencies and hence possibly also different oxide production rates for the different laser parameters (Gilbert *et al.* 2017). In a second test, we assessed the degree of plasma loading by monitoring the reduction in ^{36}Ar intensity during test ablations of the BCR-2 pellet (Gilbert *et al.* 2017). Ablating the BCR-2 pellet with the same high yield laser parameters applied to the natural materials, ^{36}Ar intensity decreased by ~ 8% relative to the gas background. With the laser spot size reduced to 75 μm, plasma loading decreased to a ~ 3% reduction. In both test cases ThO/Th and UO/U stayed the same at 0.090% and 0.050% respectively. Note, these values are higher than those listed in Table 3 because this test was conducted at the beginning of a different session.

Table 3.
Oxide production and normalised ablation yields in different matrices. Ablation yield is expressed as Si sensitivity (^{29}Si intensity/reference Si mass fraction) normalised to the BCR-2 nano-powder pellet

Material	ThO/Th	UO/U	Ablation yield normalised to BCR-2 pellet
BCR-2 powder pellet	0.049	0.033	1.00
BCR-2Ga glass	0.044	0.033	0.92
NIST SRM 614 glass	0.078	0.050	1.16
02D6 MORB glass	N.M.	N.M.	0.78
Olivine crystal blank	N.M.	N.M.	1.21
Quartz pellet blank	N.M.	N.M.	0.23

N.M. = Not measured.

This test result suggests that although a degree of plasma loading occurred during the high-yield ablations, this should not have affected oxide production rates and our interference corrections. Plasma loading nevertheless opens the possibility that vaporisation, atomisation and ionisation efficiencies could have been different between high and reduced yield ablations (Table 1). For this reason, it was important to match the ablation parameters between the samples and at least one of the calibration materials, while still minimising the amount of Au introduced into the system. This is the main reason for matching the ablation parameters for NIST SRM 614 with the natural samples, and NIST SRM 612 with the synthetic glasses (Table 1).

Results

Interference production rates

Interference production rates expressed as % (intensity/intensity) are summarised in Table 2. The HfOH and TaO interferences amounted to corrections on ^{197}Au of $< 1\%$ for all the synthetic NIST and USGS glasses, 2–10% for the MORB materials, and 20–40% for the relatively Hf–Ta rich and Au-poor BHVO-2, BCR-2 and AGV-2 pellets. The Hf and Ta related corrections were often of a similar magnitude, demonstrating the importance of applying both. The ZrO interference amounted to corrections on ^{107}Ag of $< 1\%$ for all the synthetic glasses and 10–50% for the natural materials. Tests measuring both Ag isotopes showed that mass fractions derived from uncorrected ^{109}Ag were only a few per cent higher than those derived from corrected

^{107}Ag. However, locating a material to resolve the combined $^{93}Nb^{16}O$ and $^{92}Zr^{16}O^{1}H$ interferences on ^{109}Ag proved difficult as Zr is commonly present as a minor element in natural Nb minerals, including the columbite we tested. This suggests that ^{109}Ag may be a better isotope choice for avoiding interferences when measuring Nb-poor materials. However, we elected to use ^{107}Ag with a single correction, following Jenner and O'Neill (2012b).

Production rates of $^{40}Ar^{35}Cl/^{35}Cl$ measured on halite was near detection at between 0.001–0.01 %, which amounted to < 1% of the ^{75}As intensity for the material with the highest measured Cl/As intensity ratio (BIR-1). Consequently, no $^{40}Ar^{35}Cl$ corrections were applied in this study. For more As-depleted and Cl-rich materials, this interference may require correction and should still be monitored (e.g., Jenner *et al.* 2015). Production of doubly charged ($^{150}Sm^{2+}$ + $^{150}Nd^{2+}$) / ($^{150}Sm^{+}$ + $^{150}Nd^{+}$) was relatively consistent between sessions, amounting to a < 1% correction on the NIST calibration glasses, a 10–25% correction for the USGS powders and synthetic glasses and a 35–45% correction on the As-poor MORB glasses.

Blank values and limits of quantification

The suitability of the San Carlos olivine blank for correction of ablation-remobilised contamination is supported by an olivine ablation yield within ~ 20% of the other volcanic materials (Table 3). Moreover, no obvious spikes in signal intensity related to possible Au inclusions were observed (e.g., Ferraris and Lorand 2015). Negligible concentrations of Au in the San Carlos olivine and its suitability for contamination correction are further supported by the measured values for Au-poor materials 100D1 and AGV-2, which are not overcorrected to negative values, but are instead the same within uncertainty of the expected values.

Ablation-remobilised contamination measured on the San Carlos olivine blank material during Sessions 1–3 was ≤ 0.34 ng g^{-1} for Au, ≤ 0.22 ng g^{-1} for Ag, ≤ 5.5 ng g^{-1} for As, and below detection for Pt and Re (Table 4). For Session 4, which took place one year later in 2022, the ablation blank for Au was much higher at 1.60 ± 0.53 ng g^{-1}. Results from this high-blank session are only given for the synthetic glasses GSD-2G and BHVO-2G, which have Au contents orders of magnitude higher than this blank, and for JB-3 with the blank corrected Au value presented as informational. Session 4 was conducted after other sessions involving NIST SRM 610, demonstrating the vital importance of ablation blank monitoring for ultra-trace Au analysis. The following discussion of the method ablation blank and derived LOQs refer to Sessions 1–3 that better capture the performance of a relatively clean system.

Corrections for ablation-remobilised contamination amounted to < 5% for Ag and As. The correction for Au was < 1% for all the synthetic glasses, 10–30 % for the natural materials with 1–5 ng g^{-1} Au, > 30% for materials with < 1 ng g^{-1} Au, and 40% for JB-3 in Session 4. Following Pettke *et al.* (2012), median LODs calculated from the gas background for Au, Ag, Pt and Re were all < 0.04 ng g^{-1}, with As being slightly higher at 1.85 ng g^{-1} (Table 4). The LOQ determined by the level of ablation-remobilised contamination, however, was significantly higher than this for Au and As and slightly higher for Ag (Table 4).

The mean procedural blank for the nano-powder pellets determined on the synthetic quartz pellet was below the detection limit for Au, Pt and Re, and was 0.18 ± 0.04 ng g^{-1} for Ag and 50 ± 26 ng g^{-1} for As (Table 4). These procedural blank values are not corrected with the olivine blank and hence show that the nano-powder pellet production process did not substantially contaminate the powders with Au, Ag, Pt, or Re. The Si-monitored ablation yield for the quartz pellet was just 0.23 of that of the BCR-2 pellet (Table 3), partly explaining why ablation-remobilised Au contamination was not detectable with the quartz procedural blank. However, this mismatch is offset by the far more abrasive properties of quartz on the agate milling equipment than volcanic powder, which exacerbates any procedural contamination from milling (Peters and Pettke 2016). Negligible contamination with Au and the other analytes in the powder-pellet is supported by the lack of a systematic offset to higher analyte mass fractions for the reference materials prepared as nano-powder pellets (Figures 4, 5). As the olivine blank yielded a much lower As value of 3.6 ± 3.1 ng g^{-1}, remobilised system contamination cannot easily explain the 50 ± 26 ng g^{-1} As procedural blank value for the quartz pellet. This suggests the powder-pellet making process contaminated the quartz with As at a level comparable to that in some natural volcanic materials.

Corrected mass fractions

Following the interference and blank corrections described above, the mean results for the USGS powders and JB-3, prepared as nano-powder pellets, are listed in Table 5 along with comparative literature values. All reported uncertainties are 2*s* or the 95% confidence interval. Results for the glasses, not prepared as powder pellets, are reported in Table 6 for NIST SRM 616, the Reykjanes Ridge glasses and six additional USGS glass reference materials

Table 4.
Blank values and limits of quantification (LOQ) and detection (LOD) for low-blank Sessions 1–3. See Table S2 for high blank Session 4 values

Value (ng g^{-1})	Au	Ag	As	Pt	Re
Synthetic quartz pellet procedural blank (mean, n = 3)	B.D.	0.18	49.8	B.D.	B.D.
2s	-	0.04	26.1	-	-
San Carlos olivine ablation blank (mean, n = 7)	0.29	0.21	3.56	B.D.	B.D.
2s	0.09	0.22	3.12	-	-
LOQ (Mean + 2s of olivine blank)	0.38	0.43	6.68	-	-
LOD* (median)	0.017	0.27	1.85	0.036	0.013

B.D. = Below Detection; *LOD calculated after Pettke *et al.* (2012).

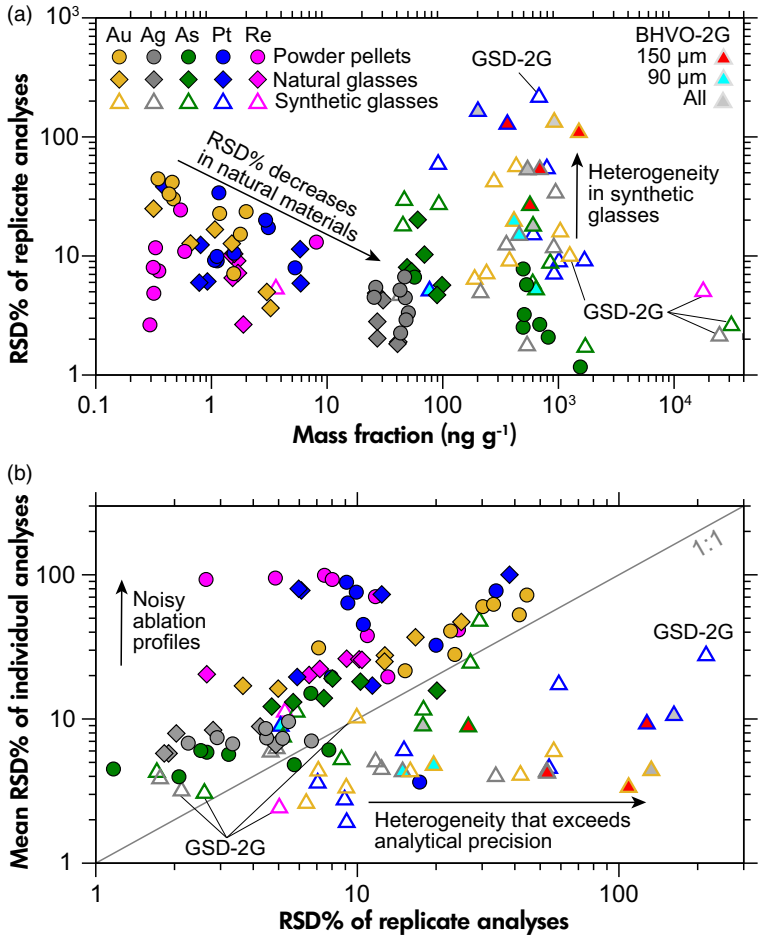

Figure 4. Precision and heterogeneity tests. (a) RSD of replicate analyses vs. mean mass fraction for each set of consecutive replicate analyses on a sample (n = 5–8), following interference and ablation blank correction and error propagation. (b) RSD of replicate analyses vs. mean RSD of each individual ablation analysis.

(BIR-1G, BIR-1Ga, BHVO-2G, BCR-2Ga, NKT-1G and GSD-2G).

Under the high-yield ablation parameters, the instrumental sensitivities achieved with NIST SRM 614 for Au and Ag were 45,000–60,000 cps per µg g^{-1}, 20,000–25,000 cps per µg g^{-1} for As and Pt and 60,000–70,000 cps per µg g^{-1} for Re. Measured intensities for Au, Pt and Re were hence relatively low in materials with < 1 ng g^{-1} and were more scattered for the nano-powder pellets relative to the

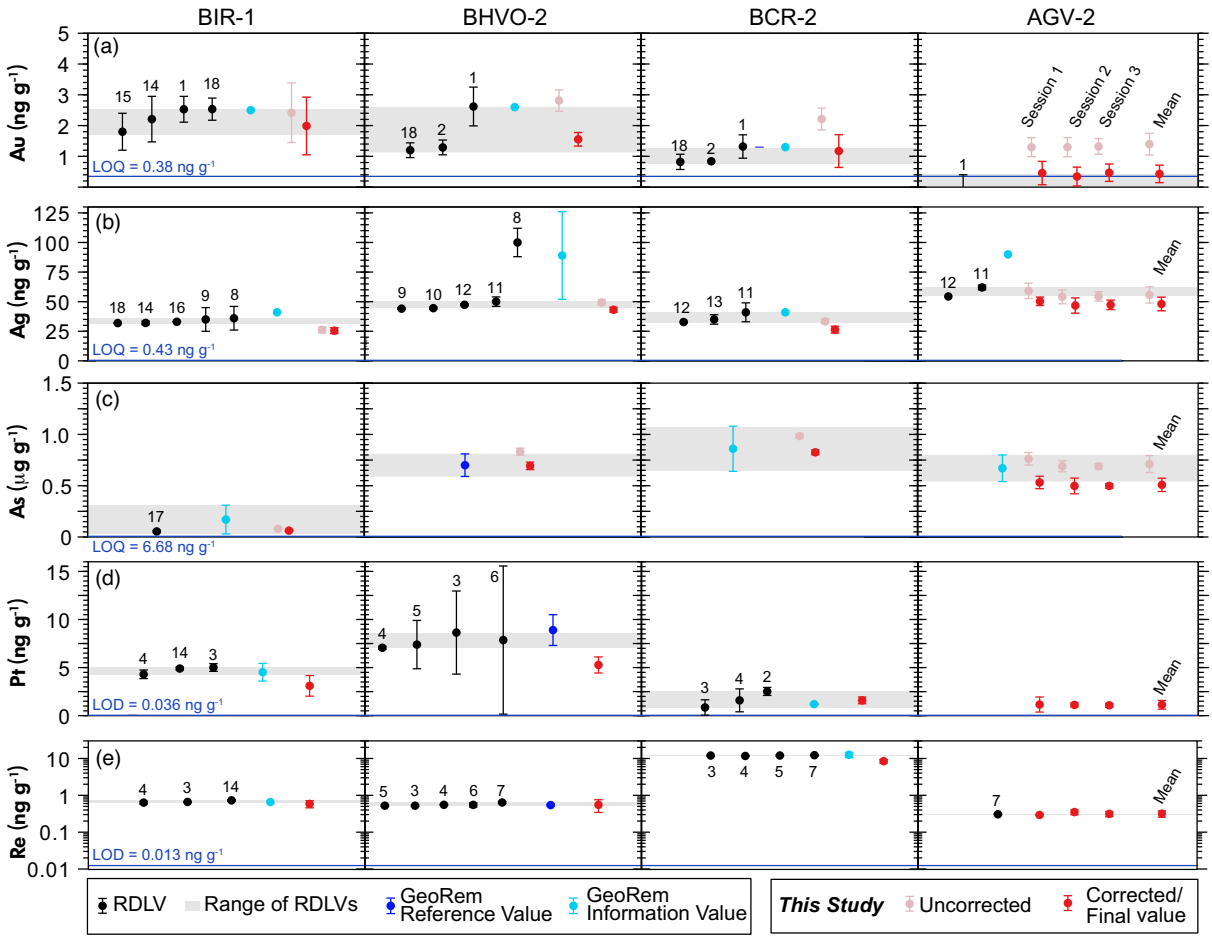

Figure 5. Mass fractions measured with LA-ICP-MS with and without interference corrections for the USGS rock powder reference materials (this study) versus previously published, rigorously determined literature values (RDLV) and the GeoReM preferred values (Jochum *et al.* 2016) for (a) gold, (b) silver, (c) arsenic, (d) platinum, (e) rhenium. The numbered references are listed in Table 5. Limits of quantification (LOQ) and limits of detection (LOD) are listed in Table 4. Range bars represent 2*s* of repeat measurements or the 95% confidence interval.

glasses, as shown by the different ablation profiles (Figure 3). This translated to higher relative standard deviation (% RSD) for both replicate and individual analyses of the powder pellets (Figure 4). Nevertheless, analyses for both materials yielded intensities above background levels for most samples and analytes.

For all the natural glasses and powder pellets, the % RSD of averaged replicate ablations is significantly lower than that calculated from individual ablation profiles (Figure 4b). This shows that, despite relatively scattered ablation signals for the powder pellets, long integration intervals and median statistics generate reproducible results. It also demonstrates the necessity of averaging at least five consecutive replicate analyses and treating this average and its standard deviation as a single result (see also Peters and Pettke 2016), to improve counting statistics and increase the sampled volume.

The AGV-2 pellet was measured sixteen times over three separate sessions as a check on the reproducibility of our interference and contamination corrections and the accuracy of calibration (Figure 5), due to its relatively low analyte/interfering element ratios. The results for AGV-2 show that even when the combined interference and contamination corrections are on the order of 50%, our determinations are internally reproducible, with a RSD including propagated ablation blank uncertainty for the sixteen ablations of 6% for

Table 5.
Results and literature values in ng g^{-1} for the rock powder reference materials

Reference material and source	Ref.	Au	2*s*	Ag	2*s*	Pt	2*s*	Re	2*s*	As	2*s*
BHVO-2											
Constantin (2009)	1	2.6	1.3								
Cheng *et al.* (2019)	2	1.29	0.24								
Cheng *et al.* (2019)	2	1.21	0.11			7.5	3.3	0.531	0.036		
Chu *et al.* (2014)	3					8.6	4.3	0.523	0.029		
Meisel and Moser (2004)	4					7.06	0.16	0.554	0.021		
Shinotsuka and Suzuki (2007)	5					7.39	2.5	0.523	0.025		
Li *et al.* (2014a)	6					7.9	7.7	0.550	0.067		
Li *et al.* (2014b)	7							0.638	0.042		
Burney *et al.* (2019)	8			100	12						
Burney *et al.* (2019)	8			100	38						
Chen *et al.* (2020)	9			44.1	0.6						
Wang *et al.* (2015)	10			44.5	0.8						
Xu *et al.* (2008)	11			50	4						
Braukmüller *et al.* (2020)	12			47.36	0.72						
GeoReM Preferred Value		(2.6)		(89)	37	8.9	1.6	0.543	0.029	700	110
RDLV Median		**1.94**		**47**		**7.49**		**0.54**			
BHVO-2 This Study (*n* = 6)		**1.56**	**0.22**	**43.2**	**1.95**	**5.27**	**0.84**	**0.54**	**0.26**	**688**	**37**
BCR-2											
Constantin (2009)	1	1.32	0.38								
Cheng *et al.* (2019)	2	0.84	0.05			2.52	0.42	12	0.3		
Cheng *et al.* (2019)	2	0.75	0.11								
Chu *et al.* (2014)	3					0.85	0.80	11.7	0.21		
Meisel and Moser (2004)	4					1.59	1.19	12.03	0.53		
Li *et al.* (2014b)	7							12.28	0.48		
Xu *et al.* (2008)	11			41	8						
Xu *et al.* (2015)	13			35	4						
Braukmüller *et al.* (2020)	12			32.78	0.64						
GeoReM Preferred Value		(1.3)		(90)		(1.2)		(12.6)		(860)	220
RDLV Median		**1.06**		**35**	**9**			**12.015**			
BCR-2 This Study (*n* = 6)		**1.17**	**0.53**	**26.3**	**2.9**	**1.57**	**0.33**	**8.1**	**2.1**	**815**	**34**
BIR-1											
Patten *et al.* (2015)	14	2.21	0.74								
Constantin (2009)	1	2.53	0.42								
Bedard and Barnes (2002)	15	1.8	0.6								
Chu *et al.* (2014)	3					5.01	0.40	0.661	0.01		
Meisel and Moser (2004)	4					4.3	0.45	0.634	0.06		
Schilling and Kingsley (2017)	14			32	1.5	4.9	0.15	0.73	0.03		
Loss (1983)	16			33	2.6						
Burney *et al.* (2019)	8			36	10						
Burney *et al.* (2019)	8			37	12						
Xu *et al.* (2008)	11			35	10						
Braukmüller *et al.* (2020)	12			31.88	0.47						
Mansur *et al.* (2020)	17									54	10
GeoReM Preferred Value		(2.5)				(4.6)	0.9	(0.065)		(170)	140
RDLV Median		**2.21**		**34**	**4**	**4.90**		**0.661**			
BIR-1 This Study (*n* = 6)		**1.99**	**0.94**	**25.5**	**2.3**	**3.1**	**1.1**	**0.59**	**0.13**	**56.9**	**7.5**
AGV-2											
Constantin (2009)	1	<0.3									
Xu *et al.* (2008)	11			62	2						
Braukmüller *et al.* (2020)	12			53.95	0.94						
Li *et al.* (2014b)	7							0.3054	0.009		
GeoReM Preferred Value				**(90)**				**(0.29)**		**(670)**	**130**
AGV-2 This Study (*n* = 16)		**0.43**	**0.29**	**48.1**	**5.6**	**1.11**	**0.44**	**0.317**	**0.061**	**506**	**65**
JB-3											
Terashima (1991)				55							
Tagami and Uchida (2001)								0.31			
Uchida *et al.* (2005)								0.30			
Imai *et al.* (1995) Compiled		**1.99**	**0.23**	**75**	**24**			**0.24**		**1840**	**240**
JB-3 This Study (*n* = 6)		**(1.77)**	**0.54**	**42.7**	**4.4**	**2.9**	**1.2**	**0.33**	**0.077**	**1544**	**36**

RDLV = Rigorously determined literature values; uncertainties are 2*s* or 95% confidence limit; figures in parentheses are information values.

As and Ag, 10% for Re, 20% for Pt, and 33% for Au. This compares with % RSD values for Au of 7–23% in other powder reference materials and 4–25% RSD for Au in the Reykjanes Ridge glasses.

Discussion

Comparison with literature values

Our results for NIST SRM 616 agree well with the GeoReM preferred values for Au, Ag, Pt and Re, but are lower than the information value for As (Jochum *et al.* 2011). This infers the accuracy of the method as applied to natural materials, but not definitively so, as the analyte/interfering element ratios in NIST SRM 616 are far higher than for the natural materials and NIST SRM 616 is matrix-matched to the calibration glasses.

More rigorous assessment of the method and potential sources of error at the ng g^{-1} level requires validation materials with natural compositions and matrices. Given the challenges of accurately measuring Au, Ag, As, Pt and Re, as well as the relatively large sample sizes required to account for the irregular distribution of Au (St. Louis 1987, Constantin 2009), it is unsurprising that the published values for the USGS reference materials have high levels of uncertainty in the GeoReM database (Jochum *et al.* 2016). For this reason, we compiled rigorously determined literature values (RDLVs) for the reference materials. These RDLVs were determined using methods that account for interferences by either chemical separation or correction and are presented alongside our values and the preferred GeoReM values for comparison (Table 5, Figure 5; Jochum *et al.* 2016). To provide a single value for comparison with this study, these literature values are calculated as the median of the reported mass fractions, with replicates within individual studies averaged into a single value.

Gold: Assessing the capability of LA-ICP-MS for determining ultra-trace Au mass fractions is the central aim of this study. The interference corrected values for Au are within uncertainty of the published values for the USGS powder and GSJ reference materials (Table 6, Figure 5). Within the range of published values, our results agree more closely with high precision solution ICP-MS determinations (Cheng *et al.* 2019, Liu *et al.* 2020, Patten *et al.* 2015) than neutron activation determinations (Constantin 2009). However, significant differences between some of the published values (e.g., BHVO-2) as well as their 2*s* uncertainties suggests either a degree of Au heterogeneity for the USGS powder reference materials at typical test portion sizes, or otherwise the influence of varying powder storage or sub-sampling techniques. Indeed, St. Louis (1987) pointed out that greater than 5 g and ideally 10 g of sample are needed for BIR-1, BHVO-1 and BCR-1 to be considered homogeneous with respect to Au. However, with depleted stocks of these reference materials, it was unfeasible to use > 2.2 g samples for this study and this may partly explain differences between the published values for Au in these materials. No Au values have previously been published for AGV-2, although Constantin (2009) reported that they were < 0.3 ng g^{-1}, which is the same within uncertainty of our near-LOQ determination of 0.43 ± 0.29 ng g^{-1}.

The Au mass fractions determined here for the Reykjanes Ridge glasses are in good agreement with published values (Webber *et al.* 2013) and within 2*s* uncertainty for all but one sample, 177D3, which was measured with 29% lower Au than previously reported (Figure 6a). Webber *et al.* (2013) determined these Au values on 4–14 g samples, which was far more material than sampled by the six ablations we made across 3–5 glass chips per sample. Heterogeneity among chips, for example caused by phenocrysts or Au-rich sulfide droplets in MORB (Patten *et al.* 2013), could explain the small differences between our microanalytical values and the bulk values previously determined (Webber *et al.* 2013).

Silver: The six literature values for Ag in BIR-1 are all in good agreement with one another. However, our interference-corrected mass fraction falls ~ 20% below their median value. For BHVO-2, our measured Ag mass fraction is within uncertainty of most of the literature values, which are all much lower than the value reported by Burney and Neal (2019) and the GeoReM information value (Figure 5). It is unclear why the interference-corrected Burney and Neal (2019) value differs from the other rigorously determined values. The Ag mass fractions determined in this study for BCR-2 and AGV-2 are within uncertainty of the lowermost literature values (e.g., Braukmüller *et al.* 2020), but are 10–20% lower than the median literature values (Figure 5, 6b). Together, these results suggest that although being comparably precise to solution ICP-MS analyses, our LA-ICP-MS method may systematically underestimate Ag contents in powder pellets by 10–20% (Figure 5, 6b). If this is the case, it is likely due to matrix-related, laser-induced elemental fraction between the NIST calibration glasses and the nano-powder pellets, as noted to some extent for many other elements (Garbe-Schönberg and Müller 2014). As the literature values for Ag in BIR-1 are in good agreement, a secondary correction could potentially be applied to the pellet results, as done by Garbe-Schönberg and Müller (2014). However, this introduces a significant risk of

reinforcing potentially erroneous reference values, so has not been applied at this stage.

There are no widely available reference glasses with suitably natural and homogeneous compositions to rigorously assess our Ag, Pt and Re measurements. To assess whether the Ag values determined for volcanic glasses by our method are plausible, we plotted Re versus Ag for the six measured Reykjanes Ridge glasses together with published values determined by isotope-dilution ICP-MS for another set of Reykjanes Ridge MORB glasses (Schilling and Kingsley 2017; Figure 7). The measured Ag–Re values fall well within the fields defined by Schilling and Kingsley (2017), lending support to our Ag and Re results for natural glasses.

Arsenic: The literature values for As in each of the USGS powder reference materials have a wide range of values, possibly reflecting some combination of sample heterogeneity and uncorrected interferences present in the large number of analyses compiled in GeoReM. Nevertheless, the As mass fractions determined in this study accurately reproduce the GeoReM preferred values for BHVO-2 and BCR-2, are the same within uncertainty for the BIR-1 and AGV-2 information values falling at the lower end of the 95% confidence interval (Figure 5, 6b), but are slightly lower than the compiled value for JB-3. Given the high potential for ArCl interference during routine solution ICP-MS involving HCl, the GeoReM information values for BIR-1, AGV-2 may be too high. This conclusion is supported by the similarly low As mass fraction of 54 $\pm$ 10 ng g^{-1} for BIR-1 determined by hydride generation atomic fluorescence spectrometry (Mansur *et al.* 2020). This result is substantially lower than many values in the GeoReM database, but is within uncertainty of the 56.9 $\pm$ 7.5 ng g^{-1} determination in this study, as well as the 46–92 ng g^{-1} values determined for the BIR-1-derived synthetic glasses (Table 6).

The As contamination predicted by the procedural quartz blank clearly does not affect the basaltic pellet results, as the tendency is towards underestimation, not overestimation of As, even for the low-level BIR-1 pellet. Similarly, no issues with As contamination were noted by Peters and Pettke (2016) using the same set of milling equipment. The results for the Reykjanes Ridge glasses are also relatively low for MORB (Jenner and O'Neill 2012a). This suggests that the As contamination of the quartz blank was related to the quartz matrix, brought about by the more abrasive character of quartz during processing, or potentially contamination carried over from a previously processed As-bearing material.

Platinum and rhenium: Mass fractions of Pt determined by LA-ICP-MS for the USGS powder reference materials either slightly underestimate (BIR-1, BHVO-2) or reproduce (BCR-2) the precisely defined ranges of literature values (Figure 5). Despite generally low intensities, our reported mass fractions for Re reproduce the precisely defined literature values remarkably well for the USGS reference materials (Figure 5, 6b), within 10% for BIR-1, BHVO-2 and AGV-2, and only falling 30% short of the relatively high reference value for BCR-2. As the reference value for Re is well above the detection limit, this suggests heterogeneity exists at the 2.2 g sample size for BCR-2. As described for Ag, the overlap between the six measured Reykjanes Ridge glasses and the Schilling and Kingsley (2017) dataset for both Re versus Ag (Figure 7a) and Re versus Pt (Figure 7b) suggests that the method can be used to determine Pt and Re mass fractions in the volcanic glasses similarly well to the powder pellets.

Comparison between the USGS nano-powder pellets and glasses

Comparison of the USGS glasses with their source powders (e.g., BIR-1G and BIR-1Ga with BIR-1, BHVO-2G with BHVO-2 and BCR-2Ga with BCR-2) highlights the well known Au, Ag and Pt contamination that is caused by melting at high temperatures in platinum crucibles (Table 6). High % RSD for replicate analyses relative to both analyte mass fractions and the precision of individual analyses demonstrates heterogeneity of Au, Ag, and Pt and in some cases As within each glass chip using a 90 μm spot size (Figure 4). To test whether this heterogeneity could be overcome using a larger spot size, additional analyses of BHVO-2 were undertaken with a 150-μm diameter laser spot size. However, rather than improving homogeneity, the RSDs for Au, Pt, Ag and As were higher for the 150 μm spots, as four out of twelve analyses intersected a domain that was highly enriched in Au, Ag and Pt and depleted in As. The RSD of the individual ablations for these glasses are mostly $<$ 10% (Figure 4b), which is substantially lower than the uncertainty in the GeoReM compiled values (Table 6). Together, this evidence confirms that, using a 90 μm spot size and the reduced-yield ablation parameters (Table 1), all of the USGS synthetic glasses apart from GSD-2G are heterogeneous with respect to Au, Ag and Pt, in general agreement with the findings of Hu *et al.* (2009) and known systematics for these elements during glass fusion in Pt crucibles (Eggins and Shelley 2002).

Rhenium was below detection for most of the USGS glasses, potentially due to the lower-yield ablation parameters combined with Re loss to the PGE crucibles (Eggins and Shelley 2002). Despite slightly elevated % RSD for As in the USGS glasses relative to the trend defined by the natural

Table 6.
Results for the Reykjanes Ridge MORB glasses compared with rigorously determined Au mass fractions for the MORB glasses (Webber 2013, Webber *et al.* 2013) and the USGS glass reference materials, compared with mostly information reference values from GeoReM (Jochum *et al.* 2011, Wilson 2018). All measured as glasses not powder pellets

Element (ng g^{-1})	Au	2*s*	n	Au	2*s*	Ag	2*s*	Pt	2*s*	Re	2*s*	As	2*s*
Reykjanes Ridge glasses	Webber *et al.* (2013)		This Study										
100D1	0.20	0.06	6	(0.32)	0.16	27.1	1.1	0.39	0.30	1.69	0.24	54	8.0
13_D2	0.54	0.12	6	0.66	0.17	26.5	2.6	0.80	0.20	1.52	0.20	61	24
02D6	0.85	0.46	7	1.07	0.36	27.1	1.5	0.92	0.11	1.67	0.30	49	8.0
78D2	1.73	0.17	5	1.50	0.38	30.4	2.6	0.78	0.09	1.88	0.10	69	14
179D3	3.21	0.6	6	3.24	0.24	40.5	1.5	5.90	0.69	1.57	0.33	89	8.0
177D3	4.26	0.32	6	3.01	0.30	41.2	1.6	5.8	1.3	1.49	0.30	98	11
Synthetic glasses	**Source**												
NIST SRM 616	GeoReM, Jochum *et al.* (2011)			189	24	48	20	1770	250	3.6	1.3	(200)	100
	This Study		3	188	24	42.7	4.0	1677	305	3.60	0.38	45	16
BIR-1G	GeoReM			(250)	740	(2300)	2400	(920)	100	(0.53)	0.07	(700)	3300
	This Study		6	238	34	212	21	917	129	B.D.	B.D.	46	27
BIR-1Ga	This Study		8	277	232	944	638	793	857	B.D.	B.D.	92	50
BHVO-2G	GeoReM			(445)	2180	(450)	410	(460)	90	(4.7)	1.3	(2830)	7100
BHVO-2G (90 μm)	This Study		14	420	324	412	155	83	68	B.D.	B.D.	620	80
BHVO-2G (150μm)	This Study		12	1501	3270	688	731	361	923	B.D.	B.D.	566	300
BHVO-2G (All)	This Study		26	919	2440	540	571	211	676	B.D.	B.D.	602	214
BCR2-Ga	This Study		9	1035	330	911	214	605	182	B.D.	B.D.	848	147
NKT-1G	GeoReM			(160)		(780)				(90)		(1620)	
	This Study		7	377	68	535	19	1010	180	B.D.	B.D.	1705	58
GSD-2G (μg g^{-1})	Wilson (2018)			1.25	0.48	23.0	7.0	5.01	0.090			29.0	14.0
	This Study		12	1.25	0.24	24.7	1.1	6.78	2.90	17.84	1.79	31.2	1.62

Values in parentheses are either information values or medians of GeoReM compiled analyses.

materials (Figure 4a), the mean measured As mass fractions in the glasses are the same within uncertainty of the USGS powder starting materials (Table 6). This similarly supports the < 100 ng g^{-1} As mass fractions determined for the BIR-1 powder by Mansur *et al.* (2020) and this study. This is consistent with the overall conclusion that As is not significantly lost or added during reference glass production but locally depleted or otherwise heterogeneous As domains are common (Eggins and Shelley 2002).

Limits of detection, quantification and precision

The median LODs calculated for ultra-trace elements Au, Pt and Re are slightly lower than the values of 0.25–1 ng g^{-1} for Au, 0.62–1 ng g^{-1} for Pt and 0.19 ng g^{-1} for Re reported by similar LA-ICP-MS methods (Sylvester and Eggins 1997, Norman *et al.* 2004, Jenner and O'Neill 2012b). We conclude that advances in LA-ICP-MS sensitivity combined with our high yield ablation parameters have improved detection limits for these analytes.

However, our results show that due to ablation-remobilised contamination, gas-background based LOD calculations do not adequately describe the lower limits of quantification for Au, Ag, or As. The LOQ calculated from the olivine ablation blank for these elements were all higher than the LOD, by an order of magnitude in the case of Au. To some extent, this is also likely to be true for other 'sticky' elements when targeted at ultra-trace levels, such as Li, B, U and Pb (Jenner and O'Neill 2012b), as it is for Cl and S (Rottier and Audétat 2019). These results demonstrate that monitoring of suitable ablation blank materials is a crucial step when targeting such elements or precious metals at the ultra-trace level by LA-ICP-MS. As many of the natural materials measured here required a ~ 10–50% correction for ablation-remobilised Au contamination, the method's accuracy and lower LOQ for Au stands to gain significantly from more rigorous cleaning protocols (e.g., Pitcairn et al. 2006b, Schlöglova et al. 2017) and better matrix-matched blank materials. Such blank materials could be produced by synthesising basaltic glasses in non-metallic crucibles.

The precision of this method is dependent on a varying combination of factors for each analyte: instrumental sensitivity, the variation and magnitude of interference and blank corrections and the homogeneity of the pellets for the rock

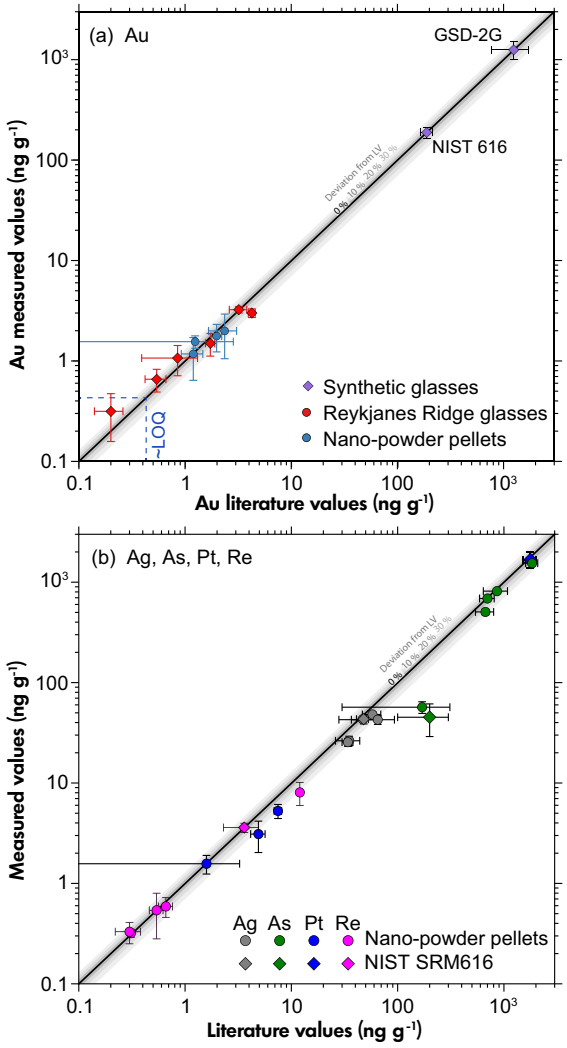

Figure 6. Measured mass fractions (this study) versus median rigorously determined literature values (LV) for (a) Au, with the Reykjanes Ridge glasses (Webber *et al.* 2013), NIST SRM 616 (Jochum *et al.* 2011), GSD-2G (Wilson 2018) and the powder reference materials in Table 5. Limit of quantification (LOQ) was calculated from the mean the San Carlos olivine blank (Table 4). (b) Ag, As, Pt, Re, all data and literature values from Table 5. The outlying Burney and Neal (2019) Ag value of 100 ng g^{-1} for BHVO-2 is excluded. Range bars represent 2*s*.

powder samples. In this study, these typically combine to RSD precisions of less than 10% for analytes above ~ 10 ng g^{-1} and less than 30% above ~ 1 ng g^{-1}, although for some samples and analytes this was significantly higher or lower (Figure 4a). Future work is required to improve the precision for low-level analytes, however the inherent reduction in precision by LA-ICPMS is a trade-off to the various advantages of laser sampling, which are discussed below.

Comparison with conventional methods and solution MS/MS

Microanalytical capability and minimal sample preparation are advantages of LA-ICP-MS that are exchanged for the disadvantages of relatively high detection limits and matrix-dependent calibration (Longerich et al. 1996, Jenner and O'Neill 2012b). Some key aspects of the LA-ICP-MS protocol presented here are compared alongside those for both well established and emerging methods for determining ultra-trace Au mass fractions in Table 7. An advantage of LA-ICP-MS is that oxide production rates are achievable at 1–2 orders of magnitude lower than conventional solution ICP-MS (Longerich et al. 1996, Jenner and O'Neill 2012b, Gilbert et al. 2017). This has gained particular relevance with the advent of whole rock nano-powder pellet analysis (Garbe-Schönberg and Müller 2014, Peters and Pettke 2016), as some elements that have traditionally been avoided due to interferences can now be measured without the need for chemical pre-separation (e.g., Au, Ag, As), as demonstrated in this study.

One apparent trade-off for the LA-ICP-MS method as applied to nano-powder pellets, is that the measured values for Ag, and possibly As and Pt calibrated with NIST glasses are often 5–25% lower than literature values determined by solution methods (Figure 5). This could be attributed to analytical uncertainty in the literature values or heterogeneity of these elements in the powder reference materials, but could also be related to laser induced elemental fraction (Jenner and O'Neill 2012b). Such laser-induced fractionation is likely to be exacerbated by the higher yield ablation parameters utilised here, and may also disproportionately affect moderately volatile elements (e.g., Ag, As; Jenner and O'Neill 2012b). Measurement at a lower laser repetition rate (e.g., 10–20 Hz) and calibration with a more closely matrix-matched basaltic glass reference material reduces such fractionation effects (Peters and Pettke 2016). However, while some basaltic reference glasses such as the USGS GSD series have suitably high, well characterised, and homogeneous As, Ag and Re mass fractions, this is not the case for Au or Pt (e.g., GSD-2G, Figure 4). For Au and Pt, NIST glasses remain the one of the only well-characterised and reasonably homogeneous calibration materials.

As an alternative or additional measure to primary calibration with a basaltic glass, secondary corrections could be applied to correct for matrix-related offsets (Garbe-Schönberg and Müller 2014). However, reference values for the analytes in this study require more certainty for this to be effective at reducing, rather than compounding error. In either case, it is important to consider spot size, ablation yield

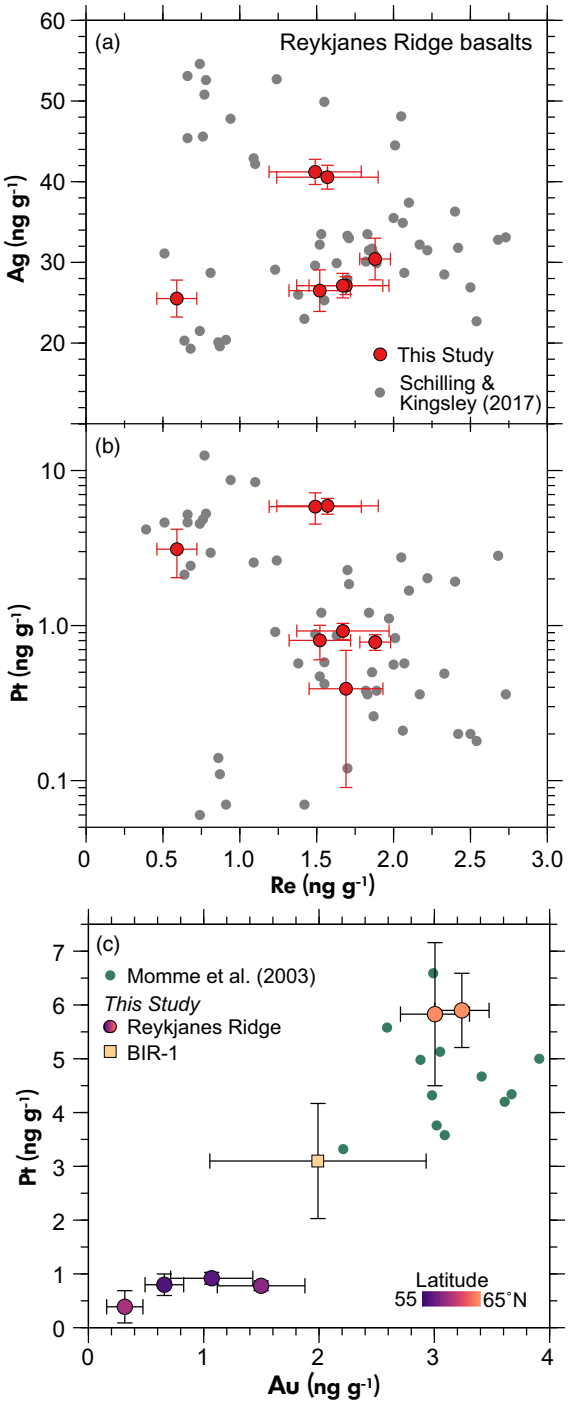

Figure 7. Comparison of Reykjanes Ridge MORB glass results from this study to rigorously determined values published for other Reykjanes Ridge and Iceland glasses and basalts (Momme *et al.* 2003, Schilling and Kingsley 2017). (a) Re versus Ag, (b) Re versus Pt, (c) Au versus Pt for the Reykjanes Ridge glasses and BIR-1 (this study) with colour mapped to recovery latitude. Range bars represent 2*s* of repeat analyses.

and the number of replicates when evaluating whether a material is sufficiently homogenous or not for calibration of each analyte (Jochum *et al.* 2011).

Ablation-remobilised contamination and the related LOQs for Au using our LA-ICP-MS system are also 2–3 orders of magnitude higher than those achievable with dedicated solution ICP-MS methods (e.g., pg g^{-1} level, Table 7; Pitcairn *et al.* 2006b, Sugiyama and Shikamori 2015, Cheng *et al.* 2019). As described by Schlöglova *et al.* (2017) for fluid inclusions and confirmed by this study for volcanic materials, reduction and correction of ablation-remobilised contamination is the main obstacle to achieving LOQs down to 0.1 ng g^{-1} for Au, Ag and As by LA-ICP-MS. The theoretical LODs suggest that reaching such levels would be possible if contamination could be sufficiently reduced and precisely corrected for (Table 4). However, a more sensitive ICP-MS instrument would likely be required to reach acceptable precisions (Figure 4a). This would extend the utility of the method to quantifying Au mass fractions in the most depleted domains of hydrothermal mineral systems (e.g., Pitcairn *et al.* 2006, Patten *et al.* 2015).

In terms of sample throughput, nano-powder pellet preparation is the slowest step in this method as applied to rock powders. An experienced user can produce around 10 pellets per day, and depending on ablation chamber capacity, can measure thirty to ninety pellets per day. Whether this throughput is a significant improvement on solution ICP-MS largely depends on whether nano-powder pellets are prepared regardless for major and trace element determination, which is common in some laboratories and settings (e.g., Peters and Pettke 2016, Rospabé *et al.* 2022). A typical analytical workflow may involve determination of major elements by XRF, trace elements by whole rock solution ICP-MS, and precious elements by pre-concentration and solution ICP-MS. In contrast, all of these elements can be analysed with a single nano-powder pellet preparation and LA-ICP-MS system using two consecutive routines by combining the protocols of Peters and Pettke (2016) and this study. The acid-free preparation of nano-powder pellets may also be considered an important safety advantage (Peters and Pettke 2016, Rospabé *et al.* 2022).

Instruments with MS/MS capability may achieve many of the advantages of the method presented in this study by online reaction. In particular, interference removal by O_2 or H_2 reaction or collision for Au, As and Se (Yim *et al.* 2012, Reekie *et al.* 2019, Sugiyama 2021), or NH_3 reaction for Au, Ag and PGEs (Sugiyama and Shikamori 2015,

Table 7.
A comparison of key methods for determining ultra-trace Au mass fractions in geological materials

Au method	INAA	Chromatographic separation and ICP-MS	NiS Fire Assay, Te co-precipitation, and ICP-MS	*Aqua regia* extraction and ICP-MS	ICP-MS/MS with NH_3 reaction	LA-ICP-MS
Example	Constantin (2009)	Pitcairn *et al.* (2006)	Savard *et al.* (2010)	Cheng *et al.* (2019)	Sugiyama and Shikamori (2015)	This Study
Sample type	Powder	Powder	Powder	Powder	Powder	Powder or *in situ*
Analyte schedule	Au, Ag, Ir, Cd, Hg	Au	Au, Pt, Ir, Os, Re, Rh, Ru	Au, Pt, Ir, Re, Ru, Pd	Au, Ag, Pt, Ir, Rh, Ru, Pd	Au, Ag, As, Pt, Re
Digestion or homogenisation method	1–3 g powder measured directly	HF–*aqua regia* digestion	NiS bead fusion and HCl dissolution	*Aqua regia* Carius tube extraction	Untested but suitable for whole rock digests	Planetary ball milling
Au pre-separation step?	Not required	Chromatographic resin extraction	NiS fusion and Te co-precipitation	*Aqua regia* extraction	Not required	Not required
Method assessment	Diverse igneous, sedimentary, ore RMs	Diverse igneous, sedimentary, ore RMs	Diverse igneous and ore RMs	Ultramafic, mafic, sediment RMs	Synthetic solutions with Au, Hf, Ta	Mafic to intermediate igneous RMs
Au instrumental detection limit (ng g^{-1})	0.3–3	0.002	-	0.0008	0.0011	0.017*
Au method blank +3*s* detection limit for whole rock samples (ng g^{-1})	0.3–3	0.010	0.48	0.009	-	0.43**

*LOD according to Pettke *et al.* (2012). **Calculated from mean ablation blank.

Hammond *et al.* 2021) are viable alternatives. For whole-rock studies an ICP-MS/MS method would likely be preferable due to superior detection limits and no need for solid reference, blank and interference monitoring materials (Table 7). However, for natural volcanic glasses and existing nano-powder pellets, an LA-ICP-MS method is advantageous. On the system used in this study, the sensitivity loss associated with pressurised reaction cells further meant that MS/MS methods could not be applied to LA-ICP-MS analysis of Au, Pt, or Re in typical natural glasses or volcanic rocks. For laboratories equipped with single quadrupole LA-ICP-MS instruments or which routinely use the nano-powder pellet method, the protocol presented here is a practical means by which to rapidly obtain accurate precious metal and As mass fractions alongside other major and trace elements.

Applicability for research and mineral exploration

Together with its relatively high throughput, the LOQs for this method should allow Au, Ag, As, Pt and Re to be more routinely examined in large suites of igneous samples. These elements have contrasting affinities for hydrothermal fluids and silicate and sulfide magmatic components (Patten *et al.* 2013), and hence may be used to unravel processes that fractionate these components in magmatic and ore-forming systems. For example, the small set of Reykjanes Ridge data measured here can be used to demonstrate that Pt and Au are co-enriched along the Reykjanes Ridge (Figure 7c), culminating to the north with similar Pt–Au compositions to Icelandic basalts (Momme *et al.* 2003).

The partitioning behaviour of the precious metals between different silicate and sulfide melts and minerals is also of importance to these systems. However, these metals are generally near or below detection in natural and experimentally produced silicate phases (e.g., Brenan *et al.* 2005, Patten *et al.* 2013), and may further display non-Henrian partitioning behaviour (Zhang and Li 2021), together yielding highly uncertain or only maximum partition coefficients. The sub ng g^{-1} *in situ* protocol presented here should allow such partition coefficients to be more precisely constrained.

The elements Au, Ag, As, Pt and Re are also key geochemical pathfinders for many different classes of ore deposit, and are commonly determined in soil and rock samples to enable geochemical vectoring towards ore zones (e.g., Cameron *et al.* 2004). For samples prepared as nano-powder pellets, the method presented achieves similar LOQs to the industry standard Ni-S fire assay and Te co-precipitation method (Table 7; Savard et al. 2010, Lawley *et al.* 2020). The LA-ICP-MS method further offers the advantage of circumventing potentially incomplete acid extraction of Au from silicate phases using *aqua regia* digests (Pitcairn *et al.* 2006), and once prepared and

loaded, pellets can be rapidly measured for conventional major and trace elements (Peters and Pettke 2016).

One potential barrier to wider implementation is the necessity for prior knowledge of the Ca mass fraction for internal standardisation. A modified approach, measuring the major elements and calibrating by normalisation to 100% *m/m* oxides could be applied. This should yield comparable results without significantly compromising the total integration time for the low-abundance analytes (Liu *et al.* 2008, Peters and Pettke 2016).

Conclusions

Combining and building on previous methods (Sylvester and Eggins 1997, Jenner and O'Neill 2012b, Garbe-Schönberg and Müller 2014), we present a practical protocol for LA-ICP-MS analysis of Au, Ag, As, Pt and Re that uses readily accessible reference materials. This refined method achieves sub-ng g^{-1} lower limits of quantification for Au, Ag, Pt and Re, and can be applied to igneous samples with mafic to intermediate compositions in either glass or nano-powder form. This matrix flexibility was utilised to assess the approach and potential sources of error with a combination of powder reference materials and previously measured MORB glasses.

Published results using wet-chemical methods for both rock powders and glasses could be reproduced by LA-ICP-MS with sufficient accuracy and precision for many use cases, such as detecting Au–Pt co-enrichment along the Reykjanes Ridge, from the μg g^{-1} level down to the sub ng g^{-1} level for Au, Ag, Pt and Re. A note of caution is that the LOQs for Au, Ag and As (calculated as the mean + 2*s* of the ablation blank) proved substantially higher than conventional detection limits calculated without consideration of ablation-remobilised contamination.

The accuracy, precision and quantification limits of the method stand to be further improved through the adoption of more rigorous cleaning protocols and more closely matrix-matched calibration and ablation blank materials. However, as detailed, the method presents an effective alternative to established approaches utilised by research and minerals industry laboratories for making ultra-trace determinations of precious metals in addition to major and trace elements.

Acknowledgements

We are grateful to Rex Taylor for providing the Reykjanes Ridge glasses. We also thank Robin Wolf and Thomas Pettke for their assistance wet milling the powders at the University of Bern. Thomas Pettke, Dieter Garbe-Schönberg, Barbara Kunz and Frances Jenner provided helpful advice at different stages of the study. The comments of two anonymous reviewers and handling editor Sarah Gilbert greatly improved the manuscript and were much appreciated. This research was supported by Swiss National Science Foundation (SNSF) grant no. P2BEP2-191795 to T. M. Belgrano, UKRI Grant. No. EP/T011548/1 to J.A. Milton and the Southampton Marine and Maritime Institute, University of Southampton.

Data availability statement

All data used in this article are reported in the tables of the main text and Supplementary Tables S1–S3.

References

Adam J. and Green T. (2006)
Trace element partitioning between mica- and amphibole-bearing garnet lherzolite and hydrous basanitic melt: 1. Experimental results and the investigation of controls on partitioning behaviour. **Contributions to Mineralogy and Petrology, 152**, 1–17.

Bédard L.P. and Barnes S.-J. (2002)
A comparison of N-type semi-planar and coaxial INAA detectors for 33 geochemical reference samples. **Journal of Radioanalytical and Nuclear Chemistry, 254**, 485–497.

Braukmüller N., Wombacher F., Bragagni A. and Münker C. (2020)
Determination of Cu, Zn, Ga, Ag, Cd, In, Sn and Tl in geological reference materials and chondrites by isotope dilution ICP-MS. **Geostandards and Geoanalytical Research, 44**, 733–752.

Brenan J.M., McDonough W.F. and Dalpé C. (2003)
Experimental constraints on the partitioning of rhenium and some platinum-group elements between olivine and silicate melt. **Earth and Planetary Science Letters, 212**, 135–150.

Brenan J.M., McDonough W.F. and Ash R. (2005)
An experimental study of the solubility and partitioning of iridium, osmium and gold between olivine and silicate melt. **Earth and Planetary Science Letters, 237**, 855–872.

Burney D. and Neal C.R. (2019)
Method for quantifying and removing polyatomic interferences on a suite of moderately volatile elements (Zn, Se, Rb, Ag, Cd, In, Sb, Tl, Pb and Bi) during solution-mode ICP-MS. **Journal of Analytical Atomic Spectrometry, 34**, 1856–1864.

Bussweiler Y., Giuliani A., Greig A., Kjarsgaard B.A., Petts D., Jackson S.E., Barrett N., Luo Y. and Pearson D.G. (2019)
Trace element analysis of high-Mg olivine by LA-ICP-MS – Characterization of natural olivine standards for matrix-matched calibration and application to mantle peridotites. **Chemical Geology, 524**, 136–157.

references

Cameron E.M. (1989)
Scouring of gold from the lower crust. Geology, 17, 26–29.

Cameron E.M., Hamilton S.M., Leybourne M.I., Hall G.E.M. and McClenaghan M.B. (2004)
Finding deeply buried deposits using geochemistry. Geochemistry: Exploration, Environment, Analysis, 4, 7–32.

Chen K., Rudnick R.L., Wang Z., Tang M., Gaschnig R.M., Zou Z., He T., Hu Z. and Liu Y. (2020)
How mafic was the Archean upper continental crust? Insights from Cu and Ag in ancient glacial diamictites. Geochimica et Cosmochimica Acta, 278, 16–29.

Cheng H., Wang Z., Chen K., Zong K., Zou Z., He T., Hu Z., Fischer-Gödde M. and Liu Y. (2019)
High-precision determination of gold mass fractions in geological reference materials by internal standardisation. Geostandards and Geoanalytical Research, 43, 663–680.

Chu Z., Yan Y., Chen Z., Guo J., Yang Y., Li C. and Zhan, Y. (2015)
A comprehensive method for precise determination of Re, Os, Ir, Ru, Pt, Pd concentrations and Os isotopic compositions in geological samples. Geostandards and Geoanalytical Research, 39, 151–169.

Constantin M. (2009)
Trace element data for gold, iridium and silver in seventy geochemical reference materials. Geostandards and Geoanalytical Research, 33, 115–132.

Crocket J.H., Keays R.R. and Hsieh S. (1968)
Determination of some precious metals by neutron activation analysis. Journal of Radioanalytical Chemistry, 1, 487–507.

Eggins S.M. and Shelley J.M.G. (2002)
Compositional heterogeneity in NIST SRM 610–617 glasses. Geostandards Newsletter: The Journal of Geostandards and Geoanalysis, 26, 269–286.

Ferraris C. and Lorand J.-P. (2015)
Novodneprite ($AuPb_3$), anyuiite [$Au(Pb, Sb)_2$] and gold micro- and nano-inclusions within plastically deformed mantle-derived olivine from the Lherz peridotite (Pyrenees, France): A HRTEM-AEM-EELS study. Physics and Chemistry of Minerals, 42, 143–150.

Fournelle J. (2011)
An investigation of "San Carlos Olivine": Comparing USNM-distributed material with commercially available material. Microscopy and Microanalysis, 17, 842–843.

Garbe-Schönberg D. and Müller S. (2014)
Nano-particulate pressed powder tablets for LA-ICP-MS. Journal of Analytical Atomic Spectrometry, 29, 990–1000.

Gilbert S., Olin P., Thompson J., Lounejeva E. and Danyushevsky L. (2017)
Matrix dependency for oxide production rates by LA-ICP-MS. Journal of Analytical Atomic Spectrometry, 32, 638–646.

Guillong M., Latkoczy C., Seo J.H., Günther D. and Heinrich C.A. (2008)
Determination of sulfur in fluid inclusions by laser ablation ICP-MS. Journal of Analytical Atomic Spectrometry, 23, 1581–1589.

Hammond S.J., Kunz B.E. and Jenner F.E. (2021)
Analysis of S, Se and Ag in volcanic glasses by ICP-QQQ-MS. Goldschmidt 2021 abstracts.

Hu Z., Liu Y., Li M., Gao S. and Zhao L. (2009)
Results for rarely determined elements in MPI-DING, USGS and NIST SRM glasses using laser ablation ICP-MS. Geostandards and Geoanalytical Research, 33, 319–335.

Imai N., Terashima S., Itoh S. and Ando A. (1995)
1994 compilation of analytical data for minor and trace elements in seventeen GSJ geochemical reference samples, "Igneous Rock Series". Geostandards Newsletter, 19, 135–213.

Jenner F.E. and O'Neill H.S.C. (2012a)
Analysis of 60 elements in 616 ocean floor basaltic glasses. Geochemistry Geophysics Geosystems, 13.

Jenner F.E. and O'Neill H.S.C. (2012b)
Major and trace analysis of basaltic glasses by laser-ablation ICP-MS. Geochemistry Geophysics Geosystems, 13.

Jenner F.E., Hauri E.H., Bullock E.S., König S., Arculus R.J., Mavrogenes J.A., Mikkelson N. and Goddard C. (2015)
The competing effects of sulfide saturation versus degassing on the behavior of the chalcophile elements during the differentiation of hydrous melts. Geochemistry Geophysics Geosystems, 16, 1490–1507.

Jochum K.P., Nohl U., Herwig K., Lammel E., Stoll B. and Hofmann A.W. (2005)
GeoReM: A new geochemical database for reference materials and isotopic standards. Geostandards and Geoanalytical Research, 29, 333–338.

Jochum K.P., Weis U., Stoll B., Kuzmin D., Yang Q., Raczek I., Jacob D.E., Stracke A., Birbaum K., Frick D.A. and others (2011)
Determination of reference values for NIST SRM 610–617 glasses following ISO guidelines. Geostandards and Geoanalytical Research, 35, 397–429.

Jochum K.P., Weis U., Schwager B., Stoll B., Wilson S.A., Haug G.H., Andreae M.O. and Enzweiler J. (2016)
Reference values following ISO guidelines for frequently requested rock reference materials. Geostandards and Geoanalytical Research, 40, 333–350.

references

Lawley C.J.M., Petts D.C., Jackson S.E., Zagorevski A., Pearson D.G., Kjarsgaard B.A., Savard D. and Tschirhart V. (2020)
Precious metal mobility during serpentinization and breakdown of base metal sulphide. Lithos, 354–355, 105278.

Li J., Jiang X.-Y., Xu J.-F., Zhong L.-F., Wang X.-C., Wang G.-Q. and Zhao P.-P. (2014a)
Determination of platinum-group elements and Re-Os isotopes using ID-ICP-MS and N-TIMS from a single digestion after two-stage column separation. Geostandards and Geoanalytical Research, 38, 37–50.

Li J., Zhao P.-P., Liu J., Wang X.-C., Yang A.Y., Wang G.-Q. and Xu J.-F. (2014b)
Reassessment of hydrofluoric acid desilicification in the Carius tube digestion technique for Re-Os isotopic determination in geological samples. Geostandards and Geoanalytical Research, 39, 17–30.

Liu Y., Hu Z., Gao S., Günther D., Xu J., Gao C. and Chen H. (2008)
In situ analysis of major and trace elements of anhydrous minerals by LA-ICP-MS without applying an internal standard. Chemical Geology, 257, 34–43.

Liu Y., Wang Z., Xue D., Yang Y., Li W., Cheng H., Patten C. and Wan B. (2020)
An improved analytical protocol for the determination of sub-nanogram gold in 1–2 g rock samples using GFAAS after polyurethane foam pretreatment. Atomic Spectroscopy, 41, 131–140.

Longerich H.P., Jackson S.E. and Günther D. (1996)
Inter-laboratory note. Laser ablation inductively coupled plasma-mass spectrometric transient signal data acquisition and analyte concentration calculation. Journal of Analytical Atomic Spectrometry, 11, 899–904.

Loss R.D., Rosman K.J.R. and de Laeter J.R. (1983)
Measurement of Ag, Te and Pd in 17 geochemical reference materials by mass spectrometric isotope-dilution analysis. Geostandards Newsletter, 7, 321–324.

Mansur E.T., Barnes S.-J., Savard D. and Webb P.C. (2020)
Determination of Te, As, Bi, Sb and Se (TABS) in geological reference materials and Geo*PT* proficiency test materials by hydride generation-atomic fluorescence spectrometry (HG-AFS). Geostandards and Geoanalytical Research, 44, 147–167.

Marxer F., Ulmer P. and Müntener O. (2022)
Polybaric fractional crystallisation of arc magmas: An experimental study simulating trans-crustal magmatic systems. Contributions to Mineralogy and Petrology, 177, 3.

Meisel T. and Moser J. (2004)
Platinum-group element and rhenium concentrations in low abundance reference materials. Geostandards and Geoanalytical Research, 28, 233–250.

Momme P., Óskarsson N. and Keays R.R. (2003)
Platinum-group elements in the Icelandic rift system: melting processes and mantle sources beneath Iceland. Chemical Geology, 196, 209–234.

Murton B.J., Taylor R.N. and Thirlwall M.F. (2002)
Plume–ridge interaction: A geochemical perspective from the Reykjanes Ridge. Journal of Petrology, 43, 1987–2012.

Norman M.D., Garcia M.O. and Bennett V.C. (2004)
Rhenium and chalcophile elements in basaltic glasses from Ko'olau and Moloka'i volcanoes: Magmatic outgassing and composition of the Hawaiian plume. Geochimica et Cosmochimica Acta, 68, 3761–3777.

Oguri K., Shimoda G. and Tatsumi Y. (1999)
Quantitative determination of gold and the platinum-group elements in geological samples using improved NiS fire-assay and tellurium coprecipitation with inductively coupled plasma-mass spectrometry (ICP-MS). Chemical Geology, 157, 189–197.

Palme H. and O'Neill H.S.C. (2014)
Cosmochemical estimates of mantle composition. In: Holland H.D. and Turekian K.K. (eds), Treatise on geochemistry (second edition). Elsevier (Oxford), 1–39.

Paton, C., Hellstrom, J., Paul, B., Woodhead, J. and Hergt, J. (2011)
Iolite: Freeware for the visualisation and processing of mass spectrometric data. Journal of Analytical Atomic Spectrometry, 26, 2508–2518.

Patten C., Barnes S.-J., Mathez E.A. and Jenner F.E. (2013)
Partition coefficients of chalcophile elements between sulfide and silicate melts and the early crystallization history of sulfide liquid: LA-ICP-MS analysis of MORB sulfide droplets. Chemical Geology, 358, 170–188.

Patten C.G.C., Pitcairn I.K., Teagle D.A.H. and Harris M. (2015)
Mobility of Au and related elements during the hydrothermal alteration of the oceanic crust: Implications for the sources of metals in VMS deposits. Mineralium Deposita, 51, 179–200.

Peters D. and Pettke T. (2016)
Evaluation of major to ultra trace element bulk rock chemical analysis of nanoparticulate pressed powder pellets by LA-ICP-MS. Geostandards and Geoanalytical Research, 41, 5–28.

Petrus J. and Paul B. (2021)
3D trace elements. GitHub. https://github.com/iolite-LA-ICP-MS/iolite4-python-examples/blob/8e1b19e78743c84176fe91ee326fbf0acb2b0d16/drs/3d_trace_elements.py

Pettke T., Oberli F., Audétat A., Guillong M., Simon A.C., Hanley J.J. and Klemm L.M. (2012)
Recent developments in element concentration and isotope ratio analysis of individual fluid inclusions by laser ablation single and multiple collector ICP-MS. Ore Geology Reviews, 44, 10–38.

references

Pitcairn, Iain K, Warwick, P.E., Milton, J.A. and Teagle, D.A.H. (2006)
Method for ultra-low-level analysis of gold in rocks. Analytical Chemistry, 78, 1290–1295.

Pitcairn I.K., Teagle D.A.H., Craw D., Olivo G.R., Kerrich R. and Brewer T.S. (2006)
Sources of metals and fluids in orogenic gold deposits: Insights from the Otago and Alpine schists, New Zealand. Economic Geology, 101, 1525–1546.

Reekie C.D.J., Jenner F.E., Smythe D.J., Hauri E.H., Bullock E.S. and Williams H.M. (2019)
Sulfide resorption during crustal ascent and degassing of oceanic plateau basalts. Nature Communications, 10, 82.

Rospabé M., Kourim F., Tamura A., Takazawa E., Giampouras M., Chatterjee S., Ishii K., Cooper M.J., Godard M., Carter E. and others (2022)
Ship-board determination of whole-rock (ultra-)trace element concentrations by laser ablation-inductively coupled plasma-mass spectrometry analysis of pressed powder pellets aboard the D/V Chikyu. Scientific Drilling, 30, 75–99.

Rottier B. and Audétat A. (2019)
In-situ quantification of chlorine and sulfur in glasses, minerals and melt inclusions by LA-ICP-MS. Chemical Geology, 504, 1–13.

Savard D., Barnes S.-J. and Meisel T. (2010)
Comparison between nickel-sulfur fire assay Te co-precipitation and isotope dilution with high-pressure asher acid digestion for the determination of platinum-group elements, rhenium and gold. Geostandards and Geoanalytical Research, 34, 281–291.

Schilling J.-G. and Kingsley R.H. (2017)
Platinum-group elements (PGE), Re, Ni, Cu, Ag and Cd variations along the Reykjanes Ridge and Iceland South-West Neovolcanic Rift Zone, from 50°N to 65°N: Implications on sulfide bearing PGE mantle source heterogeneities and partial melting effects. Interdisciplinary Earth Data Alliance (IEDA).

Schlöglova K., Wälle M. and Heinrich C.A. (2017)
LA-ICP-MS analysis of fluid inclusions: Contamination effects challenging micro-analysis of elements close to their detection limit. Journal of Analytical Atomic Spectrometry, 32, 1052–1063.

Shinotsuka K. and Suzuki K. (2007)
Simultaneous determination of platinum-group elements and rhenium in rock samples using isotope dilution inductively coupled plasma-mass spectrometry after cation exchange separation followed by solvent extraction. Analytica Chimica Acta, 603, 129–139.

St. Louis R.M. (1987)
Gold in BHVO-1, BIR-1, DNC-1 and BCR-1 by fire-assay preconcentration neutron activation analysis: Sample size vs. accuracy. Geostandards Newsletter, 11, 151–157.

Sugiyama N. (2021)
Attenuation of doubly charged ion interferences on arsenic and selenium by ICP-MS under low kinetic energy collision cell conditions with hydrogen cell gas. Journal of Analytical Atomic Spectrometry, 36, 294–302.

Sugiyama N. and Shikamori Y. (2015)
Removal of spectral interferences on noble metal elements using MS/MS reaction cell mode of a triple quadrupole ICP-MS. Journal of Analytical Atomic Spectrometry, 30, 2481–2487.

Sun W., Arculus R.J., Kamenetsky V.S. and Binns R.A. (2004)
Release of gold-bearing fluids in convergent margin magmas prompted by magnetite crystallization. Nature, 431, 975–978.

Sylvester P.J. and Eggins S.M. (1997)
Analysis of Re, Au, Pd, Pt and Rh in NIST glass certified reference materials and natural basalt glasses by laser ablation ICP-MS. Geostandards Newsletter: The Journal of Geostandards and Geoanalysis, 21, 215–229.

Tagami K. and Uchida S. (2001)
ICP-MS determination of Re at ultra trace levels in rock and soil samples. Journal of Analytical Atomic Spectrometry, 16, 669–671.

Tao D., Guo W., Xie W., Jin L., Guo Q. and Hu S. (2017)
Rapid and accurate determination of gold in geological materials by an improved ICP-MS method. Microchemical Journal, 135, 221–225.

Taylor R.N., Thirlwall M.F., Murton B.J., Hilton D.R. and Gee M.A.M. (1997)
Isotopic constraints on the influence of the Icelandic plume. Earth and Planetary Science Letters, 148, E1–E8.

Uchida S., Tagami K. and Tabei K. (2005)
Comparison of alkaline fusion and acid digestion methods for the determination of rhenium in rock and soil samples by ICP-MS. Analytica Chimica Acta, 535, 317–323.

Wang Z., Becker H. and Wombacher F. (2015)
Mass fractions of S, Cu, Se, Mo, Ag, Cd, In, Te, Ba, Sm, W, Tl and Bi in geological reference materials and selected carbonaceous chondrites determined by isotope dilution ICP-MS. Geostandards and Geoanalytical Research, 39, 185–208.

Webber A.P. (2013)
Hydrothermal mineral deposits and the behaviour of Au within the Earth. PhD Thesis (University of Southampton).

Webber A.P., Roberts S., Taylor R.N. and Pitcairn I.K. (2013)
Golden plumes: Substantial gold enrichment of oceanic crust during ridge-plume interaction. Geology, 41, 87–90.

Wilson S. (2018)
G-Probe 20 summary report. International Association of Geoanalysts, 13pp.

references

Xu J., Hu Z.-C., Liu, Y.-S., Hu, S.-H., Yuan H.-L. and Gao S. (2008)
Direct determination of Ag in geological samples by membrane desolvation-inductively coupled plasma-mass spectrometer. Chinese Journal of Analytical Chemistry, 36, 1493–1498.

Yang Z., Jackson S.E., Cabri L.J., Wee P., Longerich H.P. and Pawlak M. (2020)
Quantitative determination of trace level (ng g^{-1}) contents of rhodium and palladium in copper-rich minerals using LA-ICP-MS. Journal of Analytical Atomic Spectrometry, 35, 534–547.

Yim S.A., Choi M.S. and Chae J.S. (2012)
Direct determination of gold in rock samples using collision cell quadrupole ICP-MS. Journal of the American Society for Mass Spectrometry, 23, 171–178.

Zhang M. and Li Y. (2021)
Breaking of Henry's law for sulfide liquid–basaltic melt partitioning of Pt and Pd. Nature Communications, 12, 5994.

Supporting information

The following supporting information may be found in the online version of this article:

Figure S1. Hf versus Pt for all samples.

Table S1. Data table of all individual measurement results.

Table S2. Data for blank measurements.

Table S3. Interference productions rates for each measurement session.

This material is available from: http://onlinelibrary.wiley.com/doi/10.1111/ggr.12452/abstract (This link will take you to the article abstract).